Dynamical Models of Dark Energy

&

Their Background Cosmological Evolution

Natalie Hogg

MPhys Astrophysics

Institute of Mathematics, Physics and Computer Science

Aberystwyth University

2017

Abstract

Our current understanding of cosmology is best described by the standard ΛCDM model, in which the cosmological constant Λ is responsible for the accelerating expansion of the Universe– the phenomenon otherwise known as dark energy. There are, however, a number of problems with using the cosmological constant as a source for dark energy– fine tuning and the coincidence problem, amongst others– which we can resolve by considering a new type of dark energy: dynamical dark energy.

Dynamical dark energy models use a slowly rolling scalar field to achieve the observed accelerated expansion. The scalar field is also allowed to interact with the matter in the Universe. These models, and in particular, a coupled quintessence model with an exponential potential are the focus of this dissertation, where we find that there is evidence in recent observational data of a preference for dynamical dark energy instead of the cosmological constant.

Acknowledgements

Contents

CHAPTER 1

Introduction

Modern cosmology is a rich and maturing field. With the recent success of experiments such as the Hubble Space Telescope and the Planck satellite, a huge amount of accurate data about the state of the Universe both as it is now and as far back in time as the epoch of recombination has been obtained. A particularly defining moment in observational cosmology came just before the millennium, when, in 1998 and 1999, two remarkable papers were published which provided compelling evidence that the expansion of the Universe is accelerating [1, 2]. The name given to this phenomenon does much to convey the mystery which still surrounds it; we call it *dark energy*.

This dissertation is an investigation into what is known as dynamical dark energy, in which dark energy is modelled by a scalar field with a large potential at early times, leading to accelerated expansion at late times as the field rolls down the potential. These models are in direct contrast to the standard model of cosmology, known as ΛCDM, where dark energy is represented by the cosmological constant, Λ, and CDM stands for cold dark matter. As its name implies, Λ has a constant value everywhere in the Universe and at all times, whereas in dynamical dark energy the value of the scalar field changes with time.

The story of dark energy starts in 1916 with Einstein's theory of general relativity, from which the prediction of an expanding Universe first arose [3, 4]. The cosmological constant was included by Einstein to force a static solution to the field equations of general relativity, until the spring of 1929, when Hubble realised that the redshifted spectral lines from distant galaxies meant they are speeding away from us and the Universe is therefore expanding [5]. The cosmological constant was then removed from Einstein's equations and only reintroduced over seventy years later, after it was found that this expansion is accelerating. This time Λ represents the vacuum energy density of the Universe acting against gravity.

In this dissertation, we will firstly discuss in depth the mathematics needed to understand the expansion history of the Universe, including Einstein's field equations of general relativity and their predictions, followed by a look at the current observational evidence for the existence of dark energy. We will consider the standard ΛCDM model, discussing both its strengths and its flaws, before we look at how dynamical dark energy can alleviate

some of the problems associated with the cosmological constant in Chapter 3.

In Chapter 4 we will then look in detail at the evolution of various characterising parameters in four different models of dynamical dark energy, known as quintessence models. In particular, we will look at the evolution of the Hubble parameter, the matter density parameter and the equation of state of dark energy in these models. We will make comparisons of the models to both observational data and the ΛCDM model and look at constraining the initial conditions in the models to find a best–fit quintessence model. We will consider whether there is a preference in the data for dynamical dark energy instead of ΛCDM.

We will lastly give an overview of cosmological perturbation theory and look at the growth of small scale density perturbations in our best–fit quintessence model, again comparing the results with the predicted ΛCDM evolution. The final chapter is devoted to a short conclusion and summary of the work done in this project.

CHAPTER 2

The Universe in a Nutshell

In this chapter, we discuss the background cosmology needed to understand the expansion history of the Universe, as well as the observational evidence in favour of a late time accelerated expansion. To complete the discussion, we will briefly consider some arguments against the existence of dark energy and the rebuttals of those arguments. For the mathematics in this chapter, we follow the derivations given by Copeland, Sami and Tsujikawa [6] and Amendola and Tsujikawa [7]. Note that throughout this dissertation we also choose units such that $8\pi G = c = 1$.

2.1 Background Cosmology

The cosmological principle states that, on sufficiently large scales, the Universe is homogeneous and isotropic. This means that it looks the same in all directions and from all points. Local inhomogeneities do exist, for example, planets, stars and galaxies, which stem from very small density perturbations that have grown over time to the structures that we observe today. We will talk about this in more depth at the end of Chapter 4, but for now we limit ourselves to the simpler picture, in which we treat the large scale Universe as completely homogeneous and isotropic.

We can describe a four–dimensional, homogeneous and isotropic spacetime with the Friedmann–Lemaître–Robertson–Walker (FLRW) metric, given by

$$ds^2 = -dt^2 + a^2(t)\left[\frac{dr^2}{1 - Kr^2} + r^2(d\theta^2 + \sin^2\theta d\phi^2)\right], \tag{2.1}$$

where a is the cosmic scale factor as a function of the cosmic time t, and r, θ and ϕ are the comoving polar coordinates. K is a constant which describes the geometry of the spacetime as determined by the matter distribution in the Universe, with $K = 1,\ 0,\ -1$ corresponding to a closed, flat or open Universe respectively.

The cosmological dynamics which determine the expansion history of the Universe are

3

obtained by solving the Einstein equations, given by

$$R_{\mu\nu} - \frac{1}{2}g_{\mu\nu}R = T_{\mu\nu}, \tag{2.2}$$

where $R_{\mu\nu}$ is the Ricci tensor, R is the Ricci scalar, $g_{\mu\nu}$ is the metric tensor and $T_{\mu\nu}$ is the energy–momentum tensor. The left hand side of the equations describes the geometry of spacetime and the right hand side describes the energies and momenta of the matter species in the Universe.

From the (00) and (ii) components of (2.2), we can then obtain the Friedmann equations, which show how the Universe expands over time:

$$H^2 = \left(\frac{\dot{a}}{a}\right)^2 = \frac{1}{3}\rho - \frac{K}{a^2}, \tag{2.3}$$

$$\dot{H} = -\frac{1}{2}(p + \rho) + \frac{K}{a^2}, \tag{2.4}$$

where H is the Hubble parameter, a is again the cosmic scale factor, ρ is the energy density of all the species in the Universe, p is the pressure density of all the species in the Universe and where a dot denotes a derivative with respect to cosmic time. The change of the scale factor a with respect to time, $\dot{a}$, describes the expansion of the Universe.

By eliminating the $\frac{K}{a^2}$ term, we can find

$$\frac{\ddot{a}}{a} = -\frac{1}{6}(\rho + 3p). \tag{2.5}$$

We can then use (2.3) and (2.5) to find how the energy density evolves with cosmic time:

$$\dot{\rho} + 3H(\rho + p) = 0. \tag{2.6}$$

This is called the continuity equation.

We now consider the components of our Universe, by introducing the density parameters. We can express (2.3) in the form

$$\Omega_M + \Omega_K = 1, \tag{2.7}$$

where

$$\Omega_M = \frac{\rho}{\rho_{\text{crit}}}, \; \Omega_K = -\frac{K}{(aH)^2}. \tag{2.8}$$

The parameter Ω_M is a generalised component which describes the energy densities of the matter and energy components of the Universe, for example, the baryonic and non–baryonic matter plus a cosmological constant or dark energy. Later on, we will use a

subscript m to refer to the matter components only and a subscript Λ when referring to the cosmological constant. The critical density, $\rho_{\text{crit}} = 3H^2$, is the density at which the Universe is spatially flat. We will also use a subscript 0 when referring to the value of the parameters today.

The rate of change of the scale factor, $a(t)$, characterises the expansion rate of the Universe, so for accelerated expansion to occur we need its second derivative $\ddot{a}$ to be greater than zero, which means that $\rho + 3p < 0$ (from (2.5)). This implies that we require a negative pressure, since

$$\rho + 3p < 0, \tag{2.9}$$

$$\Rightarrow p < -\frac{\rho}{3}. \tag{2.10}$$

During the phase of accelerated expansion, we can assume that the Universe is dominated by the dark energy component, which in ΛCDM takes the form of the cosmological constant. The equation of state of dark energy is defined as

$$w = \frac{p}{\rho}, \tag{2.11}$$

and (2.10) implies that $w < -\frac{1}{3}$ for cosmic acceleration to occur.

The Hubble parameter H, the matter density parameter Ω_m and the equation of state w will be the main parameters considered in our investigation of dynamical dark energy, which will be discussed in detail in Chapter 4. Now we move on to examine the observational evidence in favour of the accelerating expansion of the Universe.

2.2 Observational Evidence for Dark Energy

There are a number of different observational pieces in the jigsaw that is dark energy; namely the luminosity distances of Type Ia supernovae, the predicted age of the Universe compared to the age of the oldest stars and the position of acoustic peaks in the CMB due to temperature anisotropies and baryon acoustic oscillations (BAOs). In this section we will discuss each of these in detail.

In the late 1990s, Riess et al. and Perlmutter et al. [1, 2] inferred the accelerated expansion of the Universe and hence the existence of dark energy from the redshifts of Type Ia supernovae (SN Ia). A Type Ia supernova occurs when a white dwarf is in orbit around a larger main sequence or red giant star. The white dwarf can accrete mass from its parent star up to the Chandrasekhar limit of 1.4 solar masses, above which the electron degeneracy pressure is not sufficient to resist the white dwarf's own gravity, causing it to collapse and resulting in a supernova [8]. Due to the well–defined mass limit at which this occurs, SN Ia

have a very predictable absolute magnitude which is independent of their redshift and are therefore used as standard candles. This means their distance from observers at Earth can be very accurately measured using the luminosity–distance relationship, as shown in (2.12) below:

$$m - M = 5 \log \left(\frac{d_L}{\text{Mpc}} \right) + 25, \tag{2.12}$$

where m is the apparent magnitude of the source, M is the absolute magnitude and d_L is the luminosity distance in Megaparsecs. Now, since the absolute magnitude is the same for any SN Ia, the luminosity distance as a function of redshift is found by observing the apparent magnitude of the supernova. We can then compare the observational data with the theoretically predicted luminosity distance, as given by

$$d_L = \frac{c(1 + z)}{H_0 \sqrt{\Omega_{K,0}}} \sinh \left(\sqrt{\Omega_{K,0}} \int_0^z \frac{d\tilde{z}}{E(\tilde{z})} \right), \tag{2.13}$$

where $\Omega_{K,0} = -K/(a_0 H_0)^2$ and $E(z) = H(z)/H_0$ [7]. We also note that z is the redshift, defined as

$$1 + z = \frac{\lambda_0}{\lambda} = \frac{a_0}{a}. \tag{2.14}$$

This equation tells us that the wavelength λ of light emitted by an object in an expanding universe increases proportionally to the scale factor a. The redshift z quantifies this effect.

Remembering that since $H = \dot{a}/a$, the Hubble parameter describes the expansion rate of the Universe, Equation (2.13) shows us that the luminosity distance is directly related to how fast the Universe is expanding. Riess et al. and Perlmutter et al. found that the observed distances of the SN Ias were around 10% – 15% further than the calculated values, implying an accelerated expansion rate. The WMAP data which provides strong evidence in favour of a flat Universe [9–11] also means that the geometry of the spacetime plays no part in the accelerated expansion. This conclusion has since been corroborated by a number of other experiments, for example the SuperNova Legacy Survey (SNLS), the Hubble Space Telescope and the rather cumbersomely named Equation of State: SupErNovae trace Cosmic Expansion, or ESSENCE [12–14].

The next piece of evidence for late time cosmic acceleration is the predicted age of the Universe t_0 compared to the age of the oldest stars, $t_s \approx 12$ Gyr [15]. We of course expect that $t_0 > t_s$, but this relation is not satisfied in a universe without some form of dark energy.

The age of the Universe can be found in the following way:

$$t_0 = \int_0^{t_0} dt, \tag{2.15}$$

$$= \int_0^{\infty} \frac{dz}{H(1+z)}, \tag{2.16}$$

$$= \int_0^{\infty} \frac{dz}{H_0 x [\Omega_{r,0} x^4 + \Omega_{m,0} x^3 + \Omega_{\Lambda,0} - \Omega_{K,0} x^2]^{\frac{1}{2}}}, \tag{2.17}$$

where $x(z) = 1 + z$ and $\Omega_{r,0}, \Omega_{m,0}, \Omega_{\Lambda,0}$ and $\Omega_{K,0}$ represent the present day values of the radiation, matter, dark energy (here represented by the cosmological constant) and curvature parameters, as explained previously in the paragraph following Equation (2.7).

We will firstly consider a flat, matter dominated Universe without any form of dark energy, i.e. $\Omega_{K,0} = 0$, $\Omega_{m,0} = 1$, $\Omega_{\Lambda,0} = 0$. As we mentioned, observational evidence has constrained the curvature of the Universe to be very close to flat, meaning that from now on, we will set $K = 0$. We can also ignore the contribution from radiation since the radiation dominated era is a negligibly small amount of time when we are integrating over the entire age of the Universe. This therefore means that $\Omega_{r,0} = 0$, and from (2.17) we find

$$t_0 = \frac{1}{H_0} \int_0^{\infty} \frac{dz}{(1+z)^2 [1 + \Omega_{m,0} z]^{\frac{1}{2}}}, \tag{2.18}$$

$$= \frac{2}{3H_0}, \tag{2.19}$$

where H_0 is the value of the Hubble parameter today (around 67.8 kms^{-1}Mpc^{-1} [16]). From this we find that

$$t_0 \approx 10 \, \text{Gyr}. \tag{2.20}$$

This does not satisfy $t_0 > t_s$. However, if we now repeat the calculations, this time including dark energy in the form of a non–zero cosmological constant, we find that

$$t_0 = \frac{1}{H_0} \int_0^{\infty} \frac{dz}{(1+z)[\Omega_{m,0}(1+z)^3 + \Omega_{\Lambda,0}]^{\frac{1}{2}}}, \tag{2.21}$$

$$= \frac{1}{H_0} \frac{2}{3\sqrt{\Omega_{\Lambda,0}}} \ln \left(\frac{1 + \sqrt{\Omega_{\Lambda,0}}}{\sqrt{\Omega_{m,0}}} \right), \tag{2.22}$$

where $\Omega_{m,0} + \Omega_{\Lambda,0} = 1$. Current observations approximately constrain $\Omega_{m,0} = 0.3$ and $\Omega_{\Lambda,0} = 0.7$ [16], from which we find that

$$t_0 \approx 13 \, \text{Gyr}, \tag{2.23}$$

which satisfies $t_0 > t_s$. This shows that dark energy is necessary for predicting the correct age of the Universe.

More evidence for the existence of dark energy comes from the cosmic microwave background, or CMB. The CMB is the oldest part of the sky we can observe (although gravitational wave astronomy may soon be able to probe further back in time [17, 18]) as it was the first point at which photons could freely propagate without being scattered.

The CMB was first observed in 1963 by Penzias and Wilson [19] and was thought to be at a uniform temperature across the whole sky until late 1992, when the COBE satellite found that there were in fact very small temperature anisotropies in the CMB [20]. This observation has since been confirmed by further experiments such as BOOMERanG and MAXIMA [21, 22]. These anisotropies occur due to perturbations in the coupling of the matter components in the Universe to gravity. We will look at cosmological perturbation theory again in Chapter 4; for now we limit ourselves to a broad strokes discussion of the resulting anisotropies.

Dark energy affects the CMB temperature anisotropies in two ways: by changing the position of acoustic peaks in the power spectrum and through the integrated Sachs–Wolfe (ISW) effect [23]. However, since the ISW occurs only on very large scales (i.e. larger than supercluster scales), the alteration of the acoustic peaks is generally more important and we will focus our discussion on these.

An acoustic peak can be thought of as similar to the resonant frequency of a guitar string; there is a certain preferred wavelength for sound waves in the early Universe. The position of the first acoustic peak corresponds to the anisotropies created by the small scale perturbations in the early Universe, which results in acoustic oscillations in the plasma.

The acoustic peak position is described by the multipole moment, l, and the position of the first peak, l_1, was predicted in the following way by Kamionkowski, Spergel and Sugiyama [24]:

$$l_1 \approx \frac{200}{\sqrt{\Omega_0}},$$
(2.24)

where

$$\Omega_0 = \Omega_m + \Omega_\Lambda.$$
(2.25)

From this prediction we can see that the presence of dark energy in the Universe will affect the position of the acoustic peak[1].

---

[1]Weinberg [25] argues for a less simplistic dependence of l_1 on Ω_0 for late time cosmology when $\Omega_\Lambda > \Omega_m$, but regardless of this, the dependence of the position of the acoustic peak l_1 on the presence of Ω_Λ– in other words, on dark energy– is clear.

The COBE satellite data was the first capable of corroborating the theoretical prediction of the acoustic peak positions, followed by the WMAP 3–year data. The WMAP results are shown in Figure 2.1. We can see that the data is an excellent match for the theoretical prediction, which is yet another confirmation that we share the Universe with dark energy.
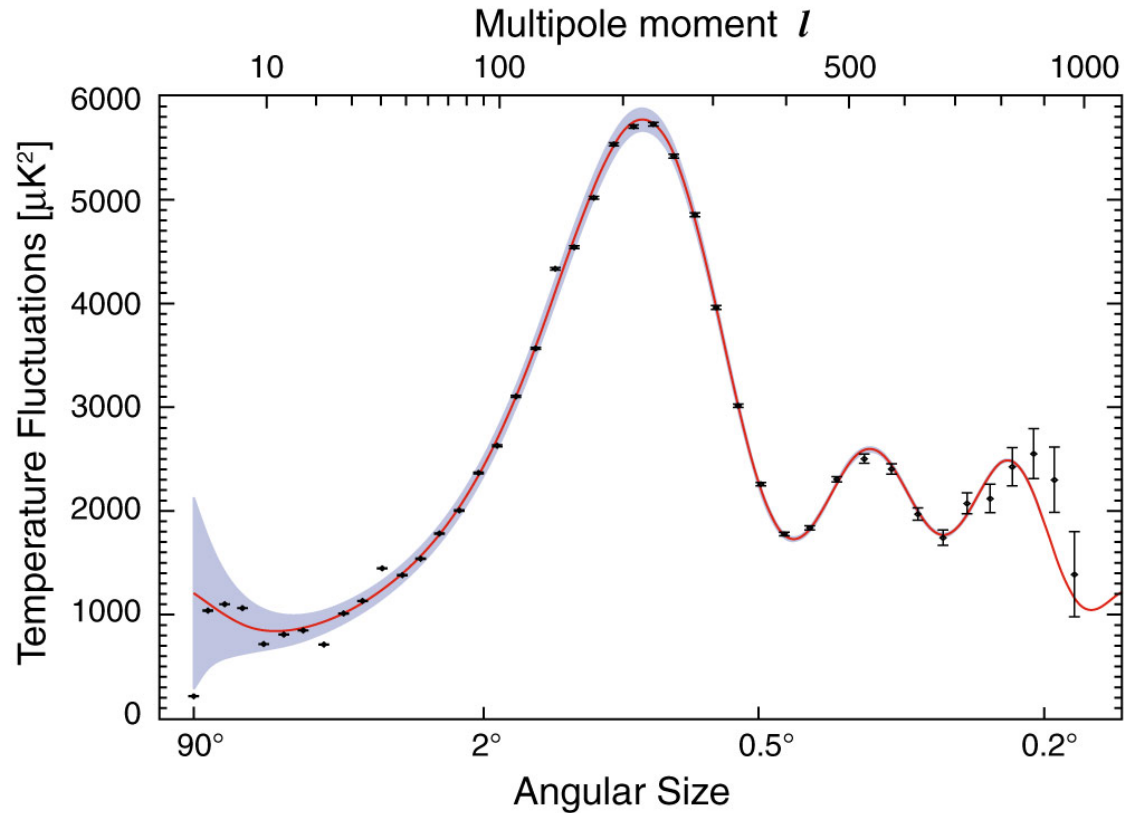
Figure 2.1: Acoustic peaks in the CMB power spectrum. The solid curve shows the theoretical prediction and the points represent the WMAP data. Reproduced from [26].

Before the recombination era, when photons decoupled from baryons and were free to propagate through the Universe, the same acoustic oscillations that caused the temperature anisotropies in the CMB also became imprinted in the baryon perturbations. These baryon acoustic oscillations, or BAOs, are another piece of evidence for the presence of dark energy. To fully understand how the observation of BAOs contributes to our observational dark energy jigsaw, we must make a brief digression, once again following the procedure laid out by Amendola and Tsujikawa [7].

We wish to theoretically predict the location of BAOs so we can compare them to observations and to do this we must consider the sound horizon where baryons were released from the Compton drag of photons. We note that this is not the same as the recombination era when photons decoupled from electrons. Compton drag is the effect of Compton scattering of CMB photons off plasma that is moving relative to the frame of the photons. The drag is analogous to a frictional force and occurs because the scattered photons remove energy from the plasma [27]. The redshift at when this occurred is called the drag epoch and is denoted by z_{drag}. The sound horizon at z_{drag} is given by

$$r_s(z_{\text{drag}}) = \int_0^{\eta_{\text{drag}}} d\eta \, c_s(\eta), \qquad (2.26)$$

where we also define the conformal time $\eta = \int a^{-1} dt$ and the sound speed c_s. To define the relative BAO distance, we must also define an effective distance

$$D_V = \left[(1+z)^2 d_L{}^2 \frac{cz}{H(z)} \right]^{\frac{1}{3}}, \qquad (2.27)$$

where d_L is the luminosity distance, as given in (2.13). The relative BAO distance is then given by

$$r_{\text{BAO}}(z) = \frac{r_s(z_{\text{drag}})}{D_V(z)}. \qquad (2.28)$$

Using a similar prediction, Percival et al. [28] plot the relative BAO distance against redshift for three different values of the cosmological constant density parameter Ω_Λ. This plot is reproduced in Figure 2.2, and we can see that the observational BAO data points favour a Universe with a non–zero cosmological constant– a Universe with dark energy.

This completes our discussion of the observational evidence in favour of an accelerating Universe– in other words, a Universe dominated by dark energy. We now move on to conclude this background chapter with a brief acknowledgement of some recent arguments against the existence of dark energy and the rebuttals of those arguments.

2.3   The Case Against Dark Energy

Despite the wealth of theoretical predictions and observational data to the contrary, there remains a small enclave of cosmologists who argue against the presence of dark energy in the Universe. Sensational news headlines are consistently generated when papers expressing such views are published (for example, [29–31]). This viewpoint is in real disagreement with the majority of cosmologists, yet, for a fair and balanced report on the state of the art, it is worth mentioning the focus of their arguments.
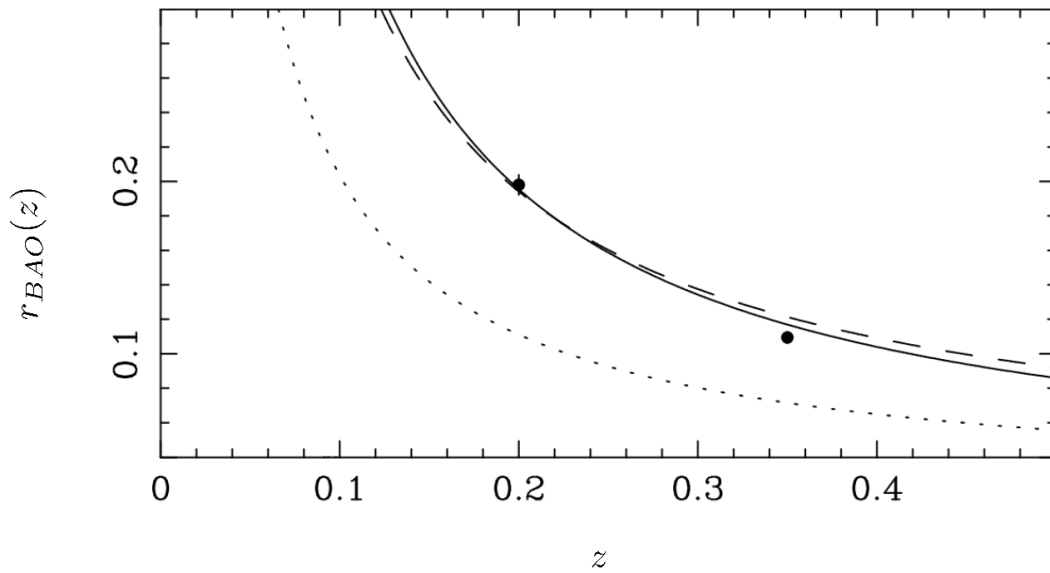
Figure 2.2: The relative BAO distance plotted against redshift for a flat universe (i.e. $\Omega_{K,0} = 0$) in three cases: the solid line indicates $\Omega_\Lambda = 0.75$, the dashed line indicates $\Omega_{m,0} = 0.3$, $\Omega_\Lambda = 0$ and the dotted line which indicates $\Omega_{m,0} = 1$, $\Omega_\Lambda = 0$. The black points show the observational data. Reproduced from [28].

The disagreement over the existence of dark energy stems mainly from the original Type Ia supernova data, as published by Riess et al. and Perlmutter et al. and discussed in section 2.2 above. In the Riess survey, data from 16 high redshift ($z > 1$) SN Ia were used, and in the Perlmutter survey, a larger sample size of 42 lower redshift (in the region of $z = 0.2 - 0.8$) were used. Many dark energy deniers argue that the datasets used are too small to draw any meaningful conclusions, but they ignore the fact that the data have been verified many times over in the twenty intervening years since the original publications; namely in the SNLS, HST and ESSENCE surveys, as previously mentioned[2].

A very recent paper by Nielsen, Guffanti and Sarkar [35] is a good example of such a claim. The authors acknowledge the increasing size of the SN Ia datasets, but then go on to state that, due to the larger amounts of data we now possess, the statistical analyses we perform on the data should be similarly improved. The authors analysed 740 SN Ia from the JLA catalogue [36] and found what they termed "marginal" evidence (i.e. $\leq 3\sigma$) for late time accelerated expansion, contrasting this with their preferred Milne model of the Universe (constant, non–accelerated expansion) [37]. However, they do then stress that the geometric evidence for an accelerated expansion (for instance, the position of the acoustic peaks in the CMB power spectrum) is inconsistent with their conclusion and requires further investigation. The assertion is then made that the SN Ia data is the best indicator of an accelerated expansion and the authors find that a modified Milne model is the best descriptor of our current Universe.

Naturally, in the months following publication of this paper, there have been a number of rebuttals published [38–41]. These papers, and in particular Rubin and Hayden [38] find that the statistical analysis performed by Nielsen, Guffanti and Sarkar has some major flaws. Rubin and Hayden produce a better statistical model which takes into account all available constraints on the data, finding that the statistical significance for an accelerating expansion becomes *more* secure, not less. This means that the SN Ia evidence for dark energy's existence is still very much valid.

To conclude this background chapter, we have covered the basic cosmology involved in the theoretical predictions for dark energy and examined in detail the observational evidence which supports the existence of dark energy. For a comprehensive discussion, we included a mention of the main argument against the existence of dark energy, and the recent rebuttals of that argument. We now move on to look at dark energy models in detail.

---

[2]It is also worth noting that some disagree with the idea of dark energy for different reasons; see [32–34] for some specific examples.

CHAPTER 3

Modelling Dark Energy

So far we have discussed some background cosmology and seen how observational evidence has been used to infer the role of dark energy as the dominant component in the Universe. We now turn to the question of what dark energy actually is, and how we can predict and model its behaviour. In this chapter, we will firstly discuss the dark energy term used in the standard model of cosmology, the cosmological constant Λ, and then look at some of the problems faced by this model. The final section of this chapter is then dedicated to a discussion of how we can solve the problems associated with the cosmological constant by invoking dynamical dark energy.

3.1 The Cosmological Constant

Recall that in section 2.1 we saw that the Einstein equations were used by Friedmann to predict an expanding Universe. However, at the time when general relativity was developed, it was believed that the Universe existed in a steady state, and would exist as such for the entirety of its history (i.e. for an infinite amount of time into the past and future).

The term Λ, representing the cosmological constant, so–called because its energy density is constant in space and time, was therefore added to the field equations of general relativity by Einstein to force a static universe solution, yielding the modified Einstein equations

$$R_{\mu\nu} - \frac{1}{2}g_{\mu\nu}R + \Lambda g_{\mu\nu} = T_{\mu\nu}, \tag{3.1}$$

which results in

$$\frac{\ddot{a}}{a} = -\frac{1}{6}(\rho + 3p) + \frac{\Lambda}{3}, \tag{3.2}$$

where Λ acts repulsively against gravity to create the static solution. This addition of Λ is often referred to as "Einstein's greatest blunder" [42], as if he had trusted his initial result

of an expanding universe, this would have been yet another powerful prediction made by the theory of general relativity.

However, the story of the cosmological constant does not end there. In the mid 1920s, Slipher found that the spectra of observed galaxies were unexpectedly redshifted [43], and a few years later, Hubble used this data to formulate his eponymous law

$$v = H_0 r, \tag{3.3}$$

where v is the recessional velocity of a galaxy and r is the distance to the galaxy, related by the value of the Hubble parameter today H_0. Hubble's law shows us that the Universe is expanding and that the further away a galaxy is, the greater its velocity away from us. Consequently, Λ was removed from the Einstein equations, only returning at the turn of the century to account for the newly discovered late–time *accelerated* expansion. While ΛCDM is undoubtedly the simplest model of the Universe we have, any such model should be tested and challenged. As mentioned, the model does have a number of problems associated with it, which motivate alternative models of dark energy. We will now discuss these problems and the alternatives in detail.

3.2   The Problem with Λ

There are many comprehensive reviews on the topic of the cosmological constant problem on which this section draws and to which the interested reader is directed, for instance [44–46]. The main attraction of using the cosmological constant as a source for dark energy is its simplicity; its energy density is constant for all times and at any place in the Universe. This energy density is postulated to originate from the vacuum; it is the vacuum energy density caused by quantum fluctuations (also known as the Casimir effect [47]). The main problem with this idea is known as the fine tuning problem. In order to have an accelerated expansion consistent with what we observe today, we require the cosmological constant to be of the same order as the Hubble parameter squared:

$$\Lambda \approx H_0^2 = 10^{-42} \text{ GeV}^2, \tag{3.4}$$

corresponding to an energy density

$$\rho_\Lambda = \frac{\Lambda m_{pl}^2}{8\pi} = 10^{-47} \text{ GeV}^4, \tag{3.5}$$

where m_{pl} is the Planck mass, here approximated as 10^{19} GeV [48]. However, if the predicted value of the vacuum energy density is calculated, as done by Copeland, Sami and Tsujikawa [6], it is found that

$$\rho_{vac} \approx 10^{74} \text{ GeV}^4. \tag{3.6}$$

It is immediately clear that there is a large discrepancy– 121 orders of magnitude– between the observed value of ρ_Λ and the predicted value of ρ_{vac}. This is the fine tuning problem, and is neatly summarised by the question: why is the value of the cosmological constant so small? This question is one of the reasons why we want to look for an alternative to the cosmological constant model of dark energy.

Another problem with the cosmological constant arises from consideration of the anthropic principle. This term was coined in 1973 by Carter [49] and expanded on by Barrow and Tipler in their book *The Anthropic Cosmological Principle* [50]. There are two versions of the principle: weak and strong.

The weak anthropic principle states that different values of observed physical constants are *not* all equally probable, but that their values are restricted by the requirement that they must allow carbon–based life to evolve. The strong anthropic principle goes one step further, stating that the Universe and hence the values of its physical constants *must* be such that observers exist within it at some point during its history.

The anthropic argument is hence invoked to explain why Λ has the value that it does; if it did not, life would not have been able to evolve in the Universe and hence we would not be here to measure it. It is clear why this is a problematic argument among scientists, as the principle hints at the possibility of a designed or created Universe and is seen by many as the easy way out of any serious consideration of why the Universe is the way we observe it to be. The avoidance of the anthropic principle is possible if a constant value of Λ is not required.

The final problem with the cosmological constant that we shall here discuss is known as the coincidence problem. This concerns the observed values of the matter density and vacuum energy density– in other words, the cosmological constant– in the Universe. As mentioned in section 2.2, current observations constrain these parameters to be approximately

$$\Omega_m = 0.3, \tag{3.7}$$
$$\Omega_\Lambda = 0.7. \tag{3.8}$$

The ratio between these two parameters is then

$$\frac{\Omega_m}{\Omega_\Lambda} = \frac{\rho_m}{\rho_\Lambda} \propto a^3, \tag{3.9}$$

where a is again the cosmic scale factor. This ratio naturally changes as the Universe expands; at early times, the vacuum energy was negligible in comparison to matter and radiation, while at late times matter and radiation become negligible as dark energy dominates.It is therefore also natural that there should be some kind of transition period between these two epochs– the coincidence is that this transition period is happening *right now*, when in ΛCDM there is no concrete physical reason that it should not have happened
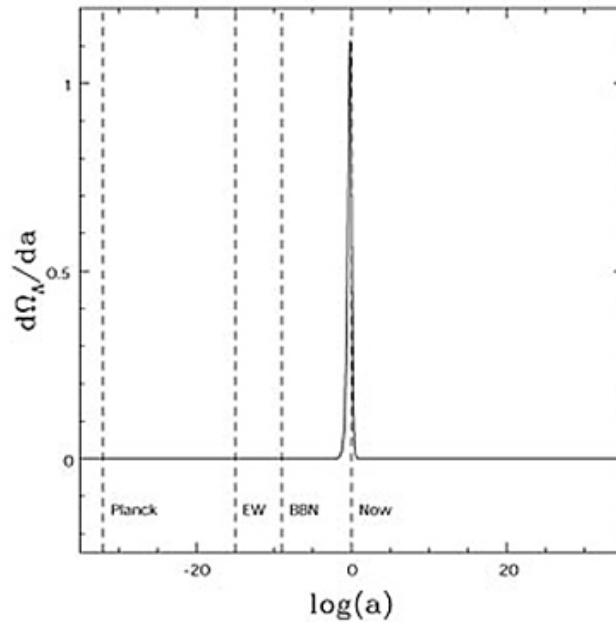
Figure 3.1: The rate of change of the vacuum energy density parameter, $d\Omega_\Lambda/da$, as a function of the scale factor a. The spike shows the coincidence of the fact that the time at which Ω_Λ is evolving is the current time. Reproduced from [51].

much earlier or later in the Universe. In Figure 3.1, the rate of change of Ω_Λ with respect to the scale factor is plotted against the logarithm of the scale factor (also known as e–foldings, which we will encounter again in Chapter 4) to show this coincidence explicitly.

However, some cosmologists (see, for example, [52–54]) do not regard the coincidence problem as a problem; an analogy used is that of the Moon being of just the right angular size on the sky that we can observe a total solar eclipse at current times. In the future, as the Moon drifts further away from the Earth and hence appears smaller, such eclipses will not be possible– yet we do not regard this as a coincidence *problem*. It is acceptable that it is just a coincidence. We note that the deliberate plotting against the *logarithm* of the scale factor in Figure 3.1 does exaggerate the coincidence, but as yet, there is no general consensus on a resolution to the coincidence problem, although dynamical dark energy in the form of a tracking quintessence model can be fine–tuned to avoid it [55].

We also note that there are further proposed difficulties with the cosmological constant arising from considerations of string theory and supersymmetry, which lie well beyond the scope of this project. For more on these topics, see, for example, [56] and [57]. While the problems mentioned above do have potential solutions within ΛCDM, the difficulties

discussed have led to many alternative models for dark energy to be proposed, in which $\Lambda = 0$ and dark energy has some other source. We will now choose one of the most popular models, quintessence, to look at in detail in the next section.

3.3 Dynamical Dark Energy

The most favoured solution to the cosmological constant problem would be a scenario in which $\Lambda = 0$, with dark energy having some alternative source that is not the constant vacuum energy density. As previously mentioned, there are a huge number of possible dark energy models and to do justice to them all would require many hundreds of pages, which is beyond the reach of this report. Therefore we will study in detail possibly one of the oldest and most well–known models: quintessence [58, 59], choosing two forms of the potential, in addition to coupling the scalar field in these models to matter. At the end of this section we will also highlight some observational and statistical evidence for dynamical dark energy.

Quintessence is a canonical scalar field ϕ, whose high potential, $V(\phi)$, at early times rolls to a low value at late times, leading to accelerated expansion. The potential only interacts with the other components of the Universe through gravity. It differs from the cosmological constant in that it has a time dependent equation of state; it is *dynamical*. Scalar fields are present in particle physics and particularly in string theory, and it is a natural continuation to introduce them into cosmology in this way. We again follow the derivations given by Copeland, Sami and Tsujikawa [6] and Amendola and Tsujikawa [7] for the mathematics in this section.

The action for quintessence is given by

$$S = \int d^4x \sqrt{-g} \left[-\frac{1}{2}(\nabla\phi)^2 - V(\phi) \right], \tag{3.10}$$

where $(\nabla\phi)^2 = g^{\mu\nu}\partial_\mu\phi\partial_\nu\phi$ and $V(\phi)$ is the potential of the field, which, as we will see, can take a number of different forms. Our flat FLRW spacetime remains the same as when we looked at the background cosmology in Chapter 2. In this background, the variation of the action with respect to ϕ yields the Klein–Gordon equation

$$\ddot{\phi} + 3H\dot{\phi} + \frac{dV}{d\phi} = 0, \tag{3.11}$$

which describes the evolution of the scalar field in time (dots once again represent cosmic time derivatives). We can also write down the energy density and pressure density of the

scalar field:

$$\rho_\phi = \frac{1}{2}\dot{\phi}^2 + V(\phi), \tag{3.12}$$

$$p_\phi = \frac{1}{2}\dot{\phi}^2 - V(\phi), \tag{3.13}$$

so that the equation of state is given by

$$w_\phi = \frac{p_\phi}{\rho_\phi} = \frac{\dot{\phi}^2 - 2V(\phi)}{\dot{\phi}^2 + 2V(\phi)}. \tag{3.14}$$

This means that in the quintessence model, Equations (2.3) and (2.5) become

$$H^2 = \frac{1}{3}\left[\frac{1}{2}\dot{\phi}^2 + V(\phi)\right], \tag{3.15}$$

$$\frac{\ddot{a}}{a} = -\frac{1}{3}\left[\dot{\phi}^2 - V(\phi)\right]. \tag{3.16}$$

We recall from (2.10) that for accelerated expansion to occur, we require that $p < -\frac{\rho}{3}$. From (3.14) we can see that for quintessence this condition means that $\dot{\phi}^2 < V(\phi)$– in other words, the accelerated expansion depends on the our choice of the potential of the scalar field.

The two forms of the potential that were studied in this project and that we will focus our discussion on are the exponential potential

$$V(\phi) = V_0 e^{-\lambda\phi}, \tag{3.17}$$

where $\lambda = -\frac{1}{V}\frac{dV}{d\phi}$, which characterises the slope of the potential through $\frac{dV}{d\phi}$; and the inverse power law potential

$$V(\phi) = V_0 \phi^{-\alpha}, \tag{3.18}$$

where the index α can take a number of arbitrary values. Our investigation into the preferred values V_0, λ and α constitutes the bulk of the novel work in this project and will be discussed fully in Chapter 4.

We also note that while in these simple models the field does not interact with matter in any way, in practice this a fairly unrealistic way to model a scalar field form of dark energy. We will therefore also consider the exponential potential and inverse power law potential with a simple non–zero coupling to the matter density, β, which represents the exchange of energy from the field to matter [60]. It is also important to note that in our investigation, we do not separate baryonic matter and dark matter– that is to say, ρ_m represents the energy density of all matter in the Universe.

When we add the coupling term, the Friedmann and continuity equations become

$$H^2 = \frac{1}{3} \left[\frac{1}{2}\dot{\phi}^2 + V(\phi) + \rho_m \right], \tag{3.19}$$

$$\dot{\rho}_m + 3H\rho_m = \beta\dot{\phi}\rho_m, \tag{3.20}$$

and the Klein–Gordon equation becomes

$$\ddot{\phi} + 3H\dot{\phi} + \frac{dV}{d\phi} = -\beta\rho_m. \tag{3.21}$$

The coupling strength, β, between matter and the scalar field is given explicitly as

$$\beta = \frac{d\ln m}{d\phi}, \tag{3.22}$$

where m is the effective particle mass [61].

The exponential potential and the inverse power law potential are of course not the only forms of quintessence that have been investigated in the literature. See, for example, [6, 7] and references therein for more on the different quintessence models.

Recall that in section 2.2 we discussed the observational evidence for the presence of dark energy in the Universe. To provide the motivation for this particular project, we should also mention the specific evidence for dynamical dark energy, of which there is a growing amount [62].

Current evidence for dynamical dark energy is mainly based on statistical analyses of available observational data. In particular, the calculation of $H(z)$ from observations of BAOs [63] (which we previously described in section 2.2) and the differential age of passively evolving galaxies (henceforth referred to as DA data) can be used to distinguish between ΛCDM and, for example, quintessence models.

The differential age technique was developed by Jimenez and Loab [64] and uses a measurement of the age difference between two galaxies at different redshifts to find the value of $\frac{dz}{dt}$. From this, $H(z)$ can then be found, using

$$H(z) = -\frac{1}{1+z}\frac{dz}{dt}. \tag{3.23}$$

Once the values of $H(z)$ have been calculated from the BAO or DA data, they can be used to determine if there is a preference for a cosmological constant or dynamical dark energy. Diagnostic tests such as the Statefinder [65] or the two point Omh^2 diagnostic were developed for this purpose by Sahni et al. [66], who found that there *is* a tension between the observed data and ΛCDM. Their diagnostic tests have since been repeated by a number

of studies [67–70], each with larger datasets, and all of these again confirm that the ΛCDM model of dark energy is not supported by the BAO and DA data.

Zhang et al. [70] in particular note that their results are weakly consistent with dynamical dark energy, but the data expected to be obtained by the upcoming DESI survey [71, 72] will be able to confirm a best fit dynamical model with a much higher level of confidence. Zheng et al. [68] also noticed that there is evidence of a strong systematic difference between the BAO and DA datasets: both datasets are individually in tension with ΛCDM, but in opposite directions. This is something we will explore further in the next chapter, when comparing the results of our investigation into quintessence with the same observational data.

To summarise this chapter, we have discussed the ΛCDM model of the Universe and the problems faced by the cosmological constant as a model of dark energy, as well as mentioning some possible resolutions to this problem. The most popular solution to the cosmological constant problem is to remove Λ entirely and replace it with a dynamical model of dark energy. We then discussed two forms of quintessence, the exponential potential and the inverse power law potential, and how the scalar field couples to matter in these models. We finally mentioned some of the observational and statistical evidence for dynamical dark energy.

We now move on to a discussion of the results of the main investigation carried out during this dissertation: whether the quintessence models mentioned above fit within the current observational constraints on the Hubble parameter H_0, the matter density parameter $\Omega_{m,0}$ and the equation of state w_0– and whether larger observational datasets indicate a preference for dynamical dark energy over ΛCDM.

CHAPTER 4

The Evolving Universe

Up until now we have largely been concerned with showing that dark energy is the dominant component in our Universe and discussing how we can model and predict its behaviour and effects. We have seen that there is a theoretical motivation for using a dynamical scalar field as the source for dark energy instead of the cosmological constant, Λ. One of the most popular models of dynamical dark energy is quintessence, in which a scalar field is the source of dark energy and the form of the potential of the field determines the expansion rate.

In this chapter we will investigate what range of values for the potential V_0, the slope of the potential λ or the power index α and the coupling strength β in both the coupled and uncoupled cases of the exponential potential and inverse power law potential quintessence models (hereafter referred to as EXPC, EXPU, IPC and IPU respectively) result in an acceptable cosmology. We then compare the results found here with the data and results described in Sahni, Shafieloo and Starobinsky, Ding et al. and Zheng et al. [66–68], to see if there is a preference in the data for a model of dynamical dark energy as an alternative to ΛCDM.

4.1 Constraining Quintessence

For this part of the project, a Python script incorporating the NumPy and SciPy modules was written to solve the Friedmann, continuity and Klein–Gordon equations for the different quintessence models. In the code, we work primarily with the e–fold number N, defined by $a = a_0 e^N$, rather than cosmic time t. We denote time derivatives with a dot (e.g. $\frac{d}{dt}\phi = \dot{\phi}$) and e–fold number derivatives with a prime (e.g. $\frac{d}{dN}\phi = \phi'$). The conversion to e–folds for any function of time $f = f(t)$ follows

$$\dot{f} = f'H, \tag{4.1}$$

which means that

$$\ddot{f} = f''H^2 + f'\dot{H}. \tag{4.2}$$

Therefore, using e–folds instead of cosmic time, equations (3.19)–(3.21) for the coupled case become

$$H^2 = \frac{\rho_m + V(\phi)}{3 - \frac{1}{2}\phi'^2}, \tag{4.3}$$

$$\rho'_m = (\beta\phi' - 3)\rho_m, \tag{4.4}$$

and

$$\phi'' = -\left(3 + \frac{\dot{H}}{H^2}\right)\phi' - \frac{V'}{H^2} - \frac{\beta\rho_m}{H^2} \tag{4.5}$$

respectively. The matter density and scalar field density parameters are given by

$$\Omega_m = \frac{\rho_m}{\rho_{\text{crit}}}, \tag{4.6}$$

$$\Omega_\phi = \frac{\frac{1}{2}(\phi'H)^2 + V}{\rho_{\text{crit}}}, \tag{4.7}$$

where ρ_{crit} is once again the critical density, $3H_0^2$. The equation of state is given by

$$w = \frac{\frac{1}{2}(\phi'H)^2 - V}{\frac{1}{2}(\phi'H)^2 + V}. \tag{4.8}$$

A sample code listing showing the integration of the background equations for the coupled exponential potential case is given in Appendix A.

4.1.1 Independent and Dependent Variables

In the models considered, we have a number of independent and dependent variables. The independent variables are the initial conditions such as ϕ and ρ_m, and the model parameters V_0, λ, α and β. The dependent variables are the results given by the code; the Hubble parameter H_0, the matter density parameter $\Omega_{m,0}$ and the equation of state w_0. The aim when running the code was to choose the independent variables such that the dependent variables found by the code were as close a match as possible to the same parameters in the observational data. We refer to this as finding an *acceptable cosmology*.

The code was written so that a range of values for the model parameters could be chosen and constraints on the initial conditions were also needed. Following Weller and Albrecht [73], the initial values for ϕ and ϕ' were set as $\phi(0) = 0.135$ and $\phi'(0) = 0$ for the exponential potential cases and $\phi(0) = 0.7$ and $\phi'(0) = 0$ for the inverse power law cases.

Some constraints on the parameters λ, α and β were also imposed. For a stable accelerating solution to be achieved, $\lambda^2 < 2$ and therefore $\lambda < \sqrt{2}$ [7]. For the inverse power law cases,

Table 4.1: This table shows the most recent Planck data for the current values of the Hubble parameter in units of $\mathrm{kms^{-1}Mpc^{-1}}$, the matter density parameter and the equation of state [16].

$H(z)$	$\Omega_{m,0}$	w_0
67.8 ± 0.9	0.308 ± 0.012	-1.006 ± 0.045

Table 4.2: This table shows the matched parameters for the exponential potential models.

Model	λ	β	V_0 ($\times 10^{-120}$)	H_0 ($\mathrm{kms^{-1}Mpc^{-1}}$)	$\Omega_{m,0}$	w_0
EXPU	0.36	0.00	0.80	67.81	0.300	-0.980
EXPC	0.23	0.01	0.76	67.80	0.300	-0.993

a natural value of α was preferred, for example, $\alpha = \frac{1}{4}, \frac{1}{3}, \frac{1}{2}$ and so on, although this was not a strict constraint and all values of α between 0.1 and 1.0 at intervals of 0.01 were checked. The coupling constant β is constrained by observations to be $\beta \leq 0.05$ [74]. When running the code, the initial redshift was set as $z = 100$, to give the solution time to settle.

It was then necessary to discard those results that did not give an acceptable cosmology– in other words, the sets of model parameters that did not result in a value of H_0, $\Omega_{m,0}$ or w_0 that matches current observational data. The data used for the matching was the most recent Planck results, given in Table 4.1. An `if/ else` statement was used to eliminate the unwanted results and the rest were written to a .csv file. When determining the best overall match, a match for H_0 was prioritised over $\Omega_{m,0}$ and w_0. The model parameters that result in the closest matches with H_0 in the Planck data are shown in Table 4.2 and Table 4.3.

It was found that the sets of model parameters that result in acceptable cosmologies number in the hundreds for EXPU and IPU and over a thousand each for EXPC and IPC, so it was firstly decided to focus only on the best matches as shown in Tables 4.2 and 4.3. We can also see from the results that, of the four models, the coupled exponential potential case provided the best overall match to the data, so we will focus on the results of that model in particular in our analysis and discussion. Furthermore, Amendola and Quercellini [75] tell us that for large values of α, the inverse power law potentials recover the exponential potential, so there is no real loss of generality if we focus only on EXPC.

Table 4.3: This table shows the matched parameters for the inverse power law potential models.

Model	α	β	V_0 ($\times 10^{-120}$)	H_0 (kms^{-1}Mpc^{-1})	$\Omega_{m,0}$	w_0
IPU	0.28	0.00	0.86	67.82	0.300	-0.987
IPC	0.33	0.05	0.88	67.79	0.320	-0.984

4.2 Comparison with Data

We have now reached the stage in our investigation where we can compare the results of the coupled exponential potential model to both the predictions of the ΛCDM model and the observational data, recalling that we want to see if there is a preference in the data for EXPC over ΛCDM. We will do this in two ways; firstly we will present and discuss some plots of the evolution of the Hubble parameter, matter density parameter and equation of state for the quintessence model and overlay observational data for a visual comparison. We will then perform a chi squared test to enable a more rigorous statistical comparison with the data to be made.

4.2.1 Plotting the Results

The first two plots, Figure 4.1 and Figure 4.2, are of the evolution of the matter density and scalar field density parameters and the evolution of the equation of state in EXPC. These were plotted to check that the quintessence model was behaving as expected, even at early times. The density parameters do evolve exactly as expected, reaching values of 0.3 and 0.7 at $z = 0$ respectively, which matches extremely well with all theoretical and observational expectations.

The evolution of the equation of state is somewhat more interesting, with the curve reaching a value of -1 at around $z = 1$, before beginning to climb again, reaching -0.993 at $z = 0$. We recall from equation (2.10) that for accelerated expansion to occur, $w < -\frac{1}{3}$, so the increasing value of w at very late times could indicate that in this model the expansion may eventually pass $w = -\frac{1}{3}$ and hence decelerate, similar to the evolution of the Universe at the end of the inflationary epoch. We stress that this is very speculative and only observations of w_0 in the distant future will allow us to determine if cosmic acceleration is ending or ongoing.

The next plot, Figure 4.3, shows the evolution of the Hubble parameter in the coupled exponential potential quintessence model and in ΛCDM. The 36 observational values of the Hubble parameter and uncertainties from Zheng et al. [68] are also shown on this plot.

The full dataset used is given in Table 4.6. This follows on from the approach taken by Sahni, Shafieloo and Starobinsky, although only two data points were used in that case. They find that the observed value of $H(z = 2.34) = 222 \pm 7$ kms^{-1}Mpc^{-1} is just outside 1σ for the value of $H(z)$ predicted by ΛCDM, as can be seen in Figure 1 of their paper [66] which we reproduce here in Figure 4.5. As we mentioned in Chapter 3, this reaffirms their assertion that the BAO data used is in tension with ΛCDM, as predicted by their use of the Omh^2 diagnostic.

The same approach was taken by Ding et al. [67], who made use of a dataset of 29 DA and BAO measurements of $H(z)$. Ding et al. also found that the tension between ΛCDM and the observed values persisted even when using the larger dataset, but were careful to point out sources of possible errors. In particular, their separate analyses of the DA and BAO data show that these data skew the tension with ΛCDM in opposite directions (see Figure 2 of [67], which we reproduce in Figure 4.6). They suggest that this may be caused by the existence of a systematic error in either the DA data or the BAO data.

Having overlaid the data in question onto Figure 4.3, it is easy to see that the inclusion of this dataset may be more of a hindrance than a help in our quest to determine a preference for either ΛCDM or EXPC, not least because of the very large uncertainties associated with most of the data. Figure 4.4 gives a closer view of the low redshift results and data (i.e. $z < 1$), but due to the very close predictions of ΛCDM and EXPC, it is still virtually impossible to tell by eye if the data is hinting at one model or the other. Therefore, to make a rigorous comparison, a chi squared test was performed, comparing the observed values of the full dataset, the DA data alone and the BAO data alone with the predicted values of ΛCDM and EXPC. The results of the chi squared test will be discussed in subsection 4.2.2.

We mentioned that Sahni, Shafieloo and Starobinsky found the value of $H(z)$ at $z = 2.34$ to be in particular tension with ΛCDM, but it is clear to see from Figure 4.3 that our prediction for ΛCDM matches this data point very well indeed. Sahni, Shafieloo and Starobinsky's statement that the Omh^2 diagnostic is independent of the value of the Hubble parameter today is correct, but in our case the predicted values of $H(z)$ in ΛCDM *do* depend on the value of H_0, due to the way the code is written. The discrepancy between Sahni, Shafieloo and Starobinsky's tension with ΛCDM at $z = 2.34$ and our matching of ΛCDM at the same redshift arises from their use of $H_0 = 70$ kms^{-1}Mpc^{-1}, in contrast with our use of $H_0 = 67.8$kms^{-1}Mpc^{-1}. Therefore it seems that the tension with the specific point at $z = 2.34$ is very much dependent on which value of H_0 we take as gospel.

This is a problem, because there are yet more disagreements between the observed values of H_0 found by different techniques and telescopes. Somewhat ironically, the worst culprit is the Hubble Space Telescope itself. The most recent measurements of H_0 by HST were found to be 71.9 kms^{-1}Mpc^{-1} and 73.0 kms^{-1}Mpc^{-1}, which strongly contrast with the most recent Planck satellite and SDSS BOSS measurements of 67.8 kms^{-1}Mpc^{-1} and 67.6 kms^{-1}Mpc^{-1} respectively [16, 76–78]. While this tension is again thought to be caused by

some systematic error, and a very recent paper by Di Valentino et al. shows it is possibly resolvable if dynamical dark energy is invoked [79], it makes matching the predicted values of EXPC (or any other quintessence model) to the observed values somewhat arbitrary, as in a year or two, an improved value for H_0 may be found, and the matching process will begin all over again.

However, we can see that a benefit of invoking models such as EXPC is that it is relatively easy to choose the model parameters so that a match to the data is achieved, and as observational constraints on H_0 improve, so too will the constraints on α, λ and β. The question will then shift to *why* these parameters are favoured over any other– and if a number of different initial values can produce the same outcome for $H(z)$ at late times, this will surely be motivation enough for dynamical dark energy, as this is similar to the inflationary models which account for the accelerated expansion in the early Universe (a large number of possible initial conditions all leading to the same result at late times) [80].

4.2.2   The Chi Squared Test

We have seen that making a visual comparison of the plots with observational data is insufficient if we wish to draw conclusions about which dark energy model best matches the data. To properly analyse the results, we perform a chi squared test. The procedure for the test runs as follows: firstly a hypothesis is stated which we wish to confirm or deny using the results of the test. The chi squared value is then calculated using

$$\chi^2 = \sum \frac{(\text{observed} - \text{expected})^2}{\text{expected}}. \tag{4.9}$$

The confidence level is then decided on, and the number of degrees of freedom (d.o.f.) calculated using

$$\text{d.o.f.} = (\text{no. of rows} - 1) \times (\text{no. of columns} - 1). \tag{4.10}$$

For example, in the case of our full dataset, as shown in Table 4.6, the number of degrees of freedom would be $(36 - 1) \times (2 - 1) = 35$. We also choose to look specifically at the 95% confidence level.

A chi squared table of values is then used to find the tabulated value corresponding to confidence level and the calculated degree of freedom [81]. The chi squared distribution is not symmetric, so there are two versions of the test: upper–tail and lower–tail. We perform an upper–tail test for the full and DA datasets and a lower–tail test for the BAO dataset. If the calculated chi squared value as found using equation (4.9) is greater than the tabulated value, in a upper–tail test the hypothesis is rejected. Conversely, when
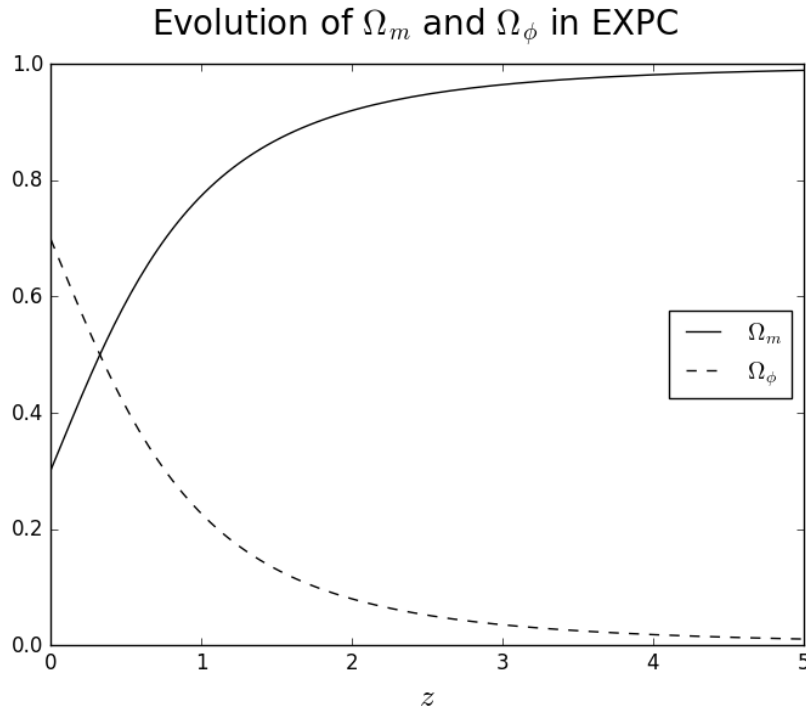
Figure 4.1: This plot shows the evolution of the matter density and scalar field density parameters in the coupled exponential potential quintessence model.
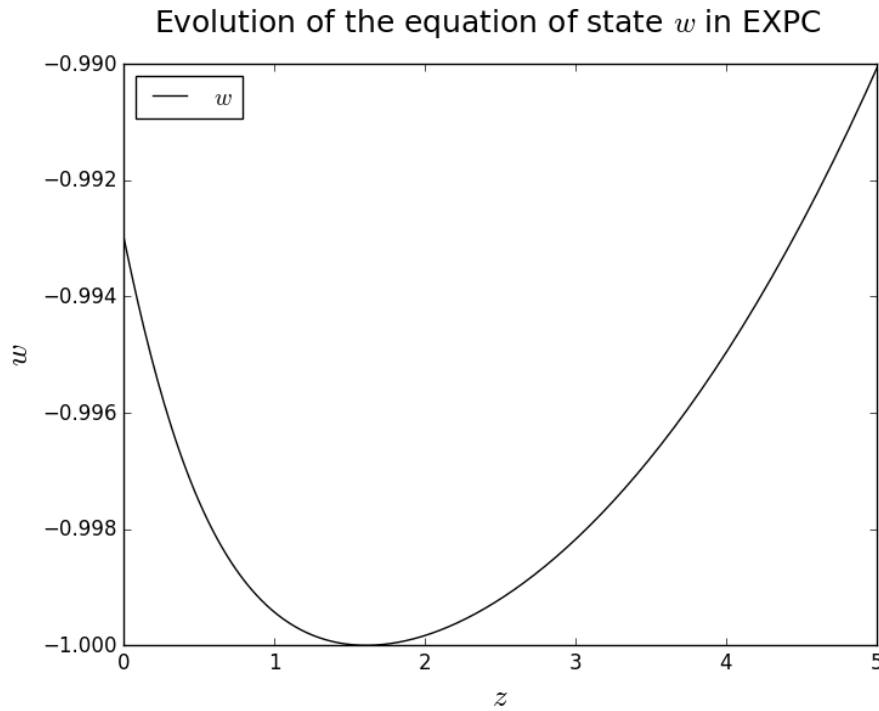

Figure 4.2: This plot shows the evolution of the equation of state in the coupled exponential potential quintessence model.
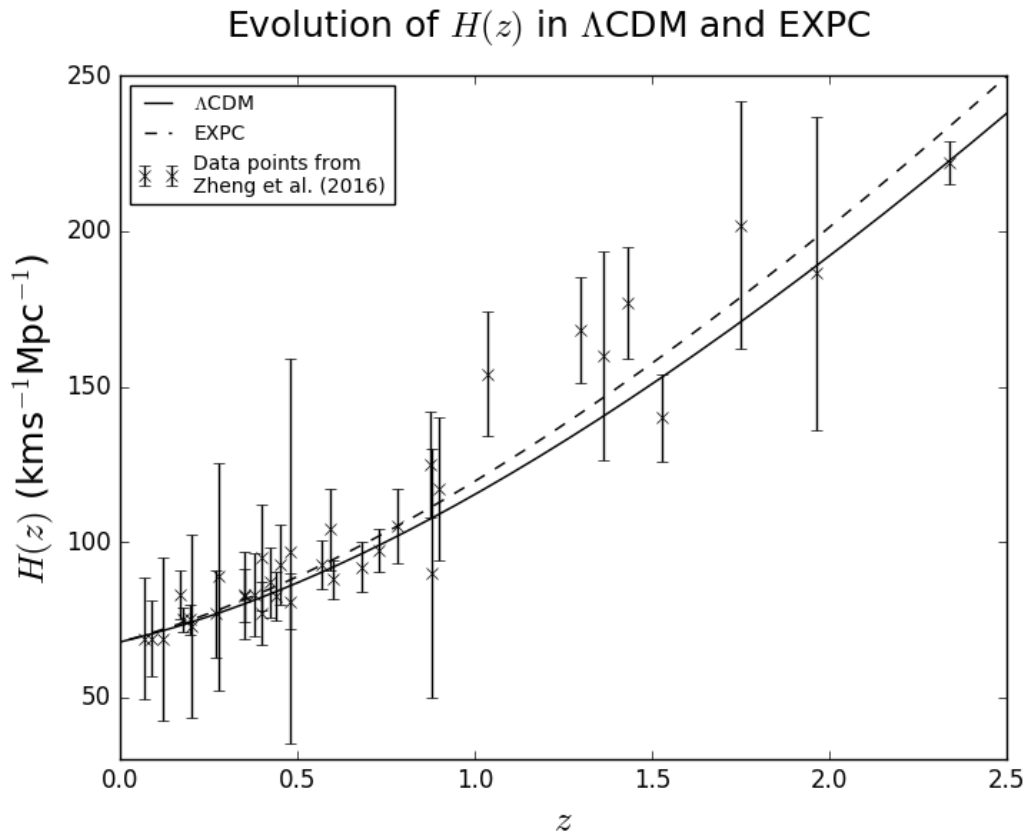
Figure 4.3: This plot shows the evolution of the Hubble parameter, $H(z)$, in ΛCDM and the coupled exponential potential quintessence model. The overlaid data points are from Zheng et al. [68] and are shown in full in Table 4.6.

## Evolution of $H(z)$ in ΛCDM and EXPC
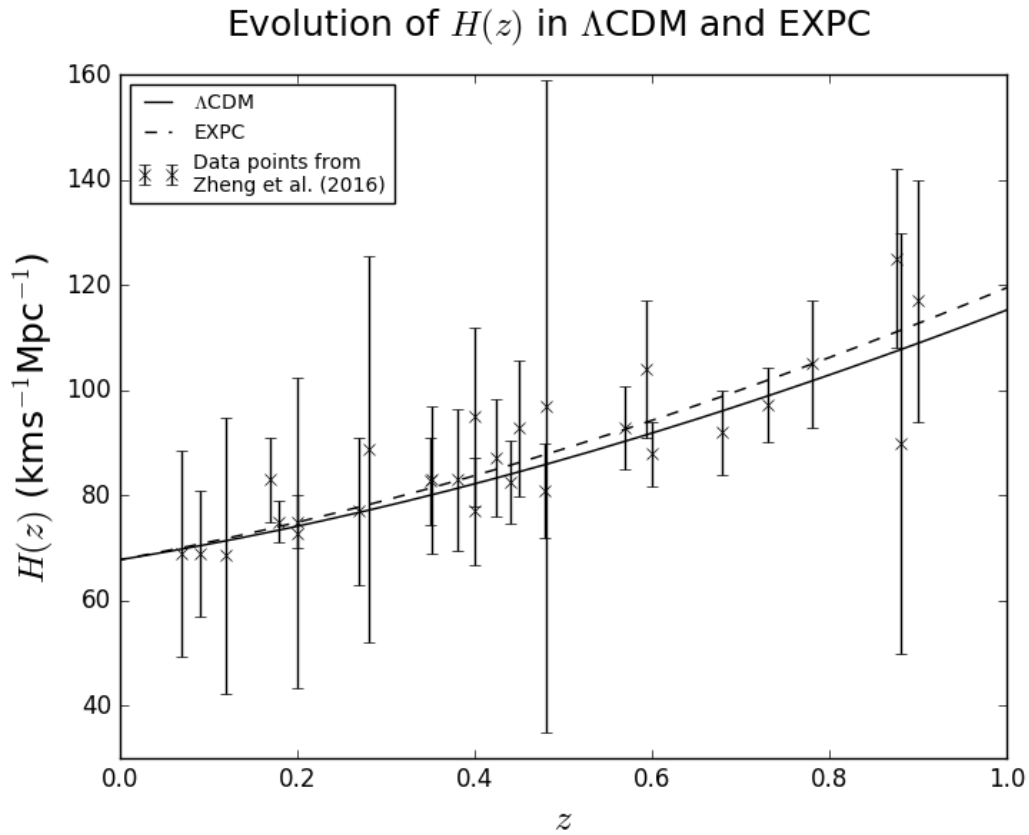
Figure 4.4: This plot shows a closer view of the evolution of the Hubble parameter, $H(z)$, in ΛCDM and the coupled exponential potential quintessence model for the low redshift results. The overlaid data points are from Zheng et al. [68] and are shown in full in Table 4.6.
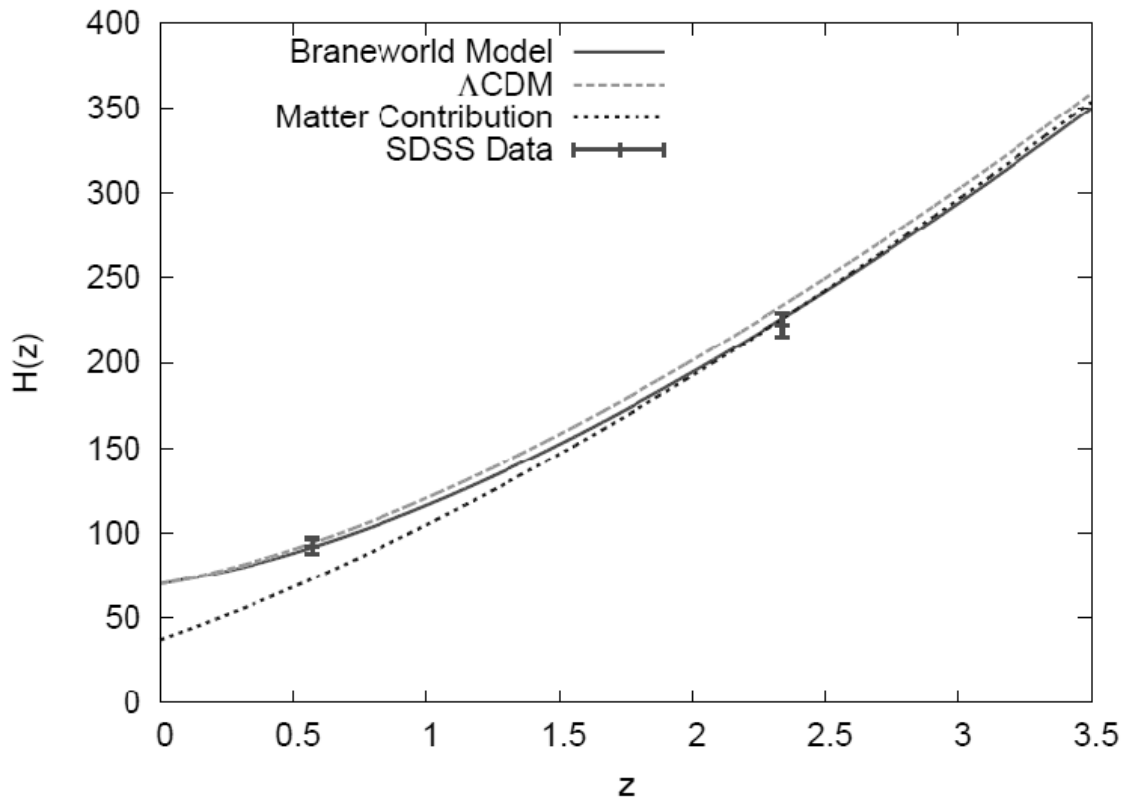
Figure 4.5: This figure is reproduced from [66] and shows the prediction of $H(z)$ in the Braneworld model favoured by Sahni, Shafieloo and Starobinsky, alongside their predictions for ΛCDM, the matter contribution $H_0\sqrt{\Omega_{m,0}(1+z)^3}$ and two SDSS data points showing the tension with ΛCDM.
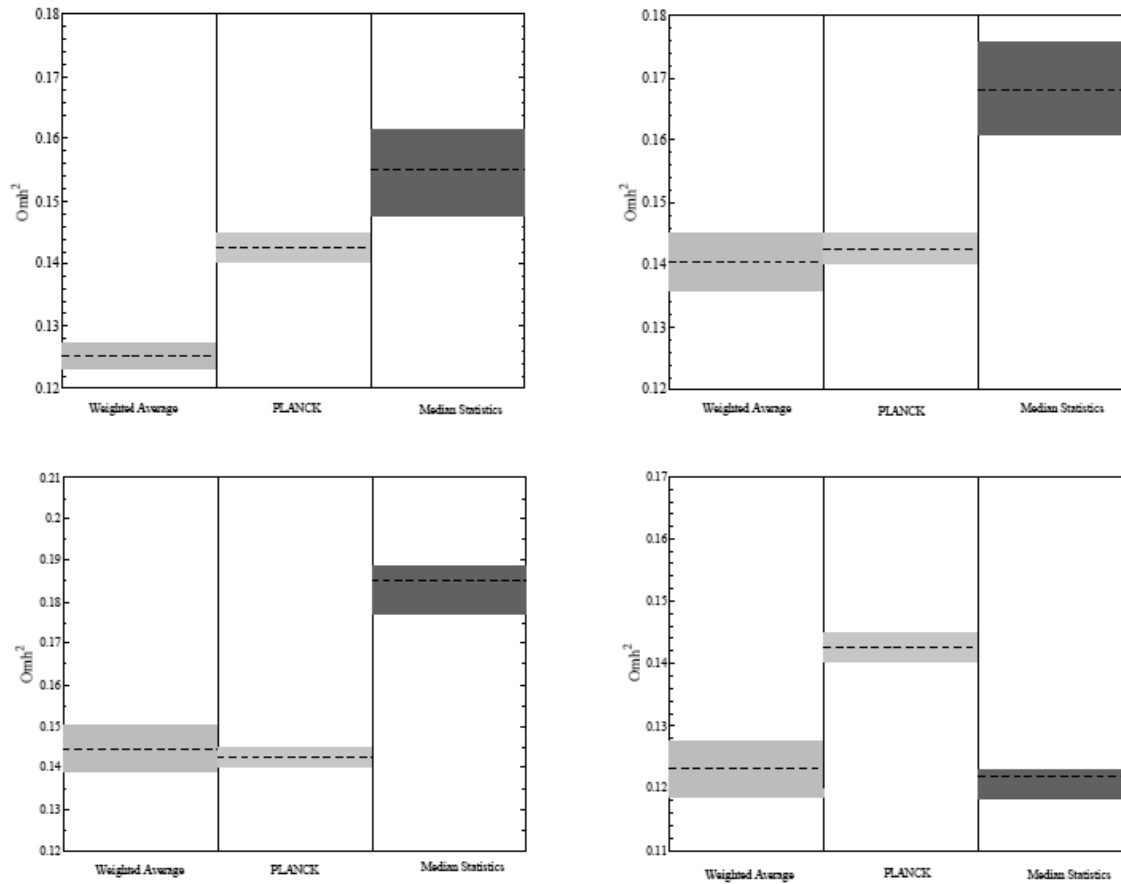
Figure 4.6: This figure is reproduced from [67] and shows the values calculated from the Omh^2 diagnostic by Ding et al. compared with the Planck data, showing how the different datasets skew the tension in different directions. The upper left plot corresponds to their full dataset of 29 data points, the upper right shows the results when the value at $z = 2.34$ point was excluded, the lower left corresponds to the DA data only and the lower right to the BAO data only.

Table 4.4: This table shows the results of the chi squared test.

Dataset	d.o.f.	Model	χ^2
Full	35	ΛCDM	52.44
		EXPC	40.86
DA only	29	ΛCDM	52.06
		EXPC	39.49
BAO only	5	ΛCDM	0.38
		EXPC	1.37

Table 4.5: This table shows the relevant critical values of the chi squared test at 95% confidence level, reproduced from [81].

d.o.f	Critical value
35	49.802
29	42.557
5	1.145

performing a lower–tail test, the hypothesis is rejected when the calculated value is *less* than the tabulated value.

A calculation of the chi squared values for both ΛCDM and EXPC was added to the Python code. These values were calculated for the full dataset in Table 4.6, as well as two reduced datasets: the DA data only and the BAO data only. These splits were made due to the evidence presented by Ding et al. that we discussed earlier: that there are some systematics at play in the DA data and hence their inclusion may skew the results. This skew would also be exaggerated due to the greater number of DA data points than BAO data points, so we will look at all the data together, as well as the two reduced datasets we described. While the chi squared test was performed for every one of the matched results generated by the sets of model parameters, due to the large number of these results we will once again only show the best match result from EXPC, although we will discuss the results of the full chi squared test. The results of the chi squared tests on the best match EXPC are shown in Table 4.4 and the relevant critical values from the chi squared distribution are given in Table 4.5.

We will look firstly at the results for ΛCDM, and state our hypothesis: *"The predicted values of $H(z)$ in ΛCDM are a good match for the observational data"*.

If we look at the value of χ^2 for the full dataset and compare it to the tabulated value,

we can see that $\chi^2_{\Lambda CDM} > \chi^2_{\text{tabulated}}$. This means that we *reject* the hypothesis. Similarly, for the DA dataset, $\chi^2_{\Lambda CDM} > \chi^2_{\text{tabulated}}$, and we again reject the hypothesis. For the BAO data, we perform a lower–tail test, meaning that for the third and final time, we reject the hypothesis, since $\chi^2_{\Lambda CDM} < \chi^2_{\text{tabulated}}$. We note that this is a fairly weak rejection, since the critical value of 1.610 at 90% confidence level means the hypothesis would be accepted.

The results for EXPC are somewhat different. Our hypothesis this time is: *"The predicted values of $H(z)$ in the coupled exponential quintessence model are a good match for the observational data"*.

For the case of the full dataset, $\chi^2_{EXPC} < \chi^2_{\text{tabulated}}$ and so we can *accept* the hypothesis. For the DA dataset, once again $\chi^2_{EXPC} < \chi^2_{\text{tabulated}}$, and for the lower–tail test on the BAO dataset, $\chi^2_{EXPC} > \chi^2_{\text{tabulated}}$, meaning that the hypothesis is accepted in all three cases.

Can we then conclude that ΛCDM should be discarded in favour of a dynamical model of dark energy such as EXPC? Unfortunately it is not that simple. While the results of our chi squared test do show a preference for EXPC over ΛCDM, we must remember that we have only shown the results of one chi squared test on one set of model parameters in EXPC. It was found that when the chi squared test was performed on every single matched result in EXPC, the full dataset and the DA dataset still showed a preference for the quintessence model, but that there was a strong preference for ΛCDM in the BAO dataset. This result is further evidence of kind of systematic error in the observational datasets.

However, our findings here are certainly food for thought. We can clearly see that if the systematic error in the DA or BAO dataset is identified and eliminated, and if more observational data is gathered, the chi squared test would be able to provide strong evidence either for or against dynamical dark energy. In this case, a faster code such as the widely used CAMB or CLASS codes [82, 83] would need to be utilised, as the large amount of data and calculations involved make the Python code written for this project very slow. We will now move on to look at the growth of small scale density perturbations in the coupled exponential potential quintessence model, and again compare this to ΛCDM.

Table 4.6: This table shows the dataset compiled by Zheng et al. [68] and used in the chi squared tests. $H(z)$ and σ_H are given in units of $\text{kms}^{-1}\text{Mpc}^{-1}$.

z	$H(z)$	σ_H	Dataset
0.07	69	19.6	DA
0.09	69	12	DA
0.12	68.6	26.2	DA
0.17	83	8	DA
0.1791	75	4	DA

z	$H(z)$	σ_H	Dataset
0.1993	75	5	DA
0.2	72.9	29.6	DA
0.27	77	14	DA
0.28	88.8	36.6	DA
0.35	82.7	8.4	BAO
0.3519	83	14	DA
0.3802	83	13.5	DA
0.4	95	17	DA
0.4004	77	10.2	DA
0.4247	87.1	11.2	DA
0.44	82.6	7.8	BAO
0.4497	92.8	12.9	DA
0.4783	80.9	9	DA
0.48	97	62	DA
0.57	92.9	7.8	BAO
0.5929	104	13	DA
0.6	87.9	6.1	BAO
0.6797	92	8	DA
0.73	97.3	7	BAO
0.7812	105	12	DA
0.8754	25	17	DA
0.88	90	40	DA
0.9	117	23	DA
1.037	154	20	DA
1.3	168	17	DA
1.363	160	33.6	DA
1.43	177	18	DA
1.53	140	14	DA
1.75	202	40	DA
1.965	186.5	50.4	DA
2.34	222	7	BAO

4.3 Cosmological Perturbation Theory

Throughout our treatment of the expanding Universe so far, we have considered it to be perfectly homogeneous. However, we know that large scale structure and therefore inhomogeneity exists in the Universe and so the question is, where did this structure come

from? The answer lies in the existence of tiny fluctuations in the initial matter density which, due to the gravitational imbalance they caused, grew rapidly in the inflationary epoch to become the large structures we observe today.

As with the rest of the Universe's expansion history, the growth of these perturbations is expected to be affected by the presence and form of dark energy. In this section we will briefly discuss how the code was modified to include the density perturbations and investigate the differences in the growth of the perturbations in ΛCDM and the coupled exponential potential quintessence model and to do this, we need to take a diversion through cosmological perturbation theory.

The evolution of the linearised density perturbations δ in ΛCDM are described by the equation [84]

$$\ddot{\delta} + 2H\dot{\delta} - \frac{1}{2}\rho_m\delta = 0, \tag{4.11}$$

This is expressed in cosmic time, but we recall that we use the e–fold number in the code, so following the conversion previously given in (4.1) and (4.2), (4.11) becomes

$$\delta'' = -2\delta' - \frac{\dot{H}}{H^2}\delta' + \frac{\rho_m\delta}{2H^2}, \tag{4.12}$$

which, since $\rho_m = 3H^2\Omega_m$, we find that

$$\delta'' = -\left(2 + \frac{\dot{H}}{H^2}\right)\delta' + \frac{3}{2}\Omega_m\delta. \tag{4.13}$$

The evolution of the density perturbations in the case of coupled dark energy such as the exponential potential quintessence are governed by the equation

$$\ddot{\delta} = -(2H + \beta\dot{\phi})\dot{\delta} + \frac{3}{2}H^2\Omega_m\delta(1 + 2\beta^2), \tag{4.14}$$

where β is the coupling strength and ϕ is the scalar field, as before. Using the e–fold number, this equation becomes

$$\delta'' = -\left(2H + \beta\phi' + \frac{\dot{H}}{H^2}\right)\delta' + \frac{3}{2}\Omega_m\delta(1 + 2\beta^2). \tag{4.15}$$

4.4 Growth of Perturbations

By using our Python code to integrate (4.13) and (4.15), we can then plot the growth factor, $\frac{\delta'}{\delta}$. Sahni, Shafieloo and Starobinsky [66] tell us that a lower value of $H(z)$ leads to faster

Evolution of density perturbations
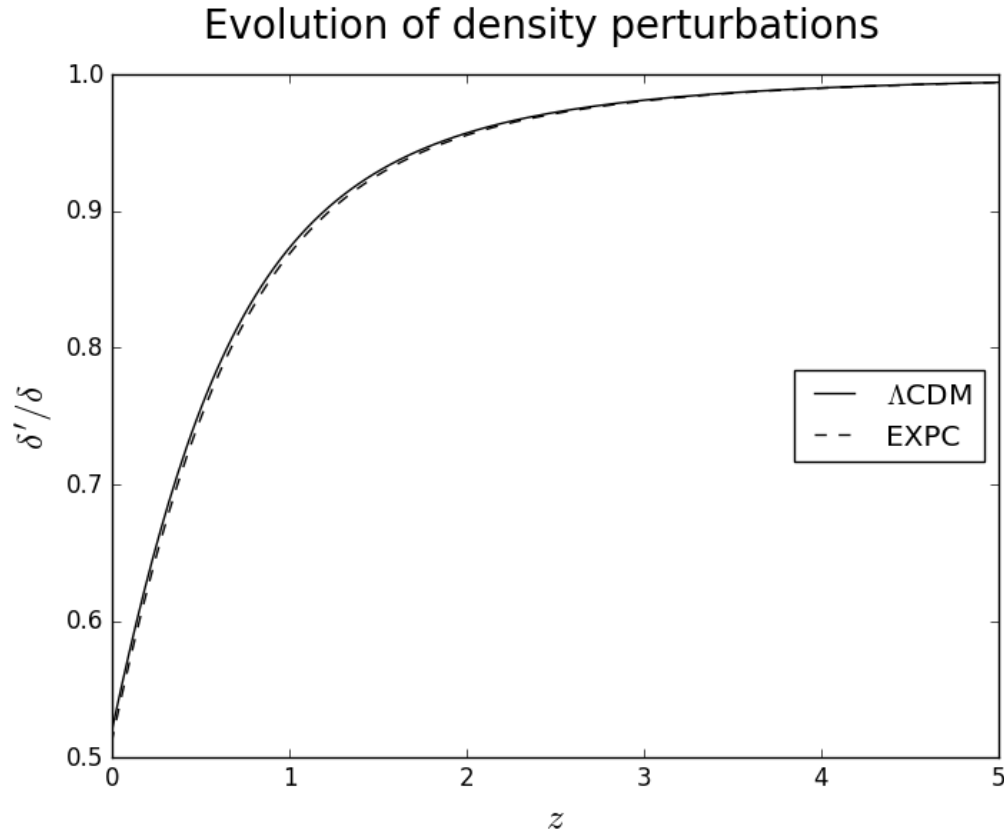
Figure 4.7: This plot shows the evolution of the growth factor $\frac{\delta'}{\delta}$ in ΛCDM and EXPC.

growth of δ than in ΛCDM, and this is indeed what we find when we plot the growth factor in Figures 4.7 and 4.8. This is confirmation that EXPC behaves exactly as expected and provides the final validation for its use as a model for dark energy.

To conclude this chapter, it is worth reiterating the key findings of our investigation. We found that a good match for observational data can be obtained by a coupled exponential potential quintessence model and a chi squared test indicates that this is a better match than that achieved by ΛCDM. This finding should be taken with a pinch of salt, due to the possible presence of systematic errors in the observational data, as mentioned by a number of other authors. We also confirmed that the growth of density perturbations is faster in EXPC than in ΛCDM, as expected.
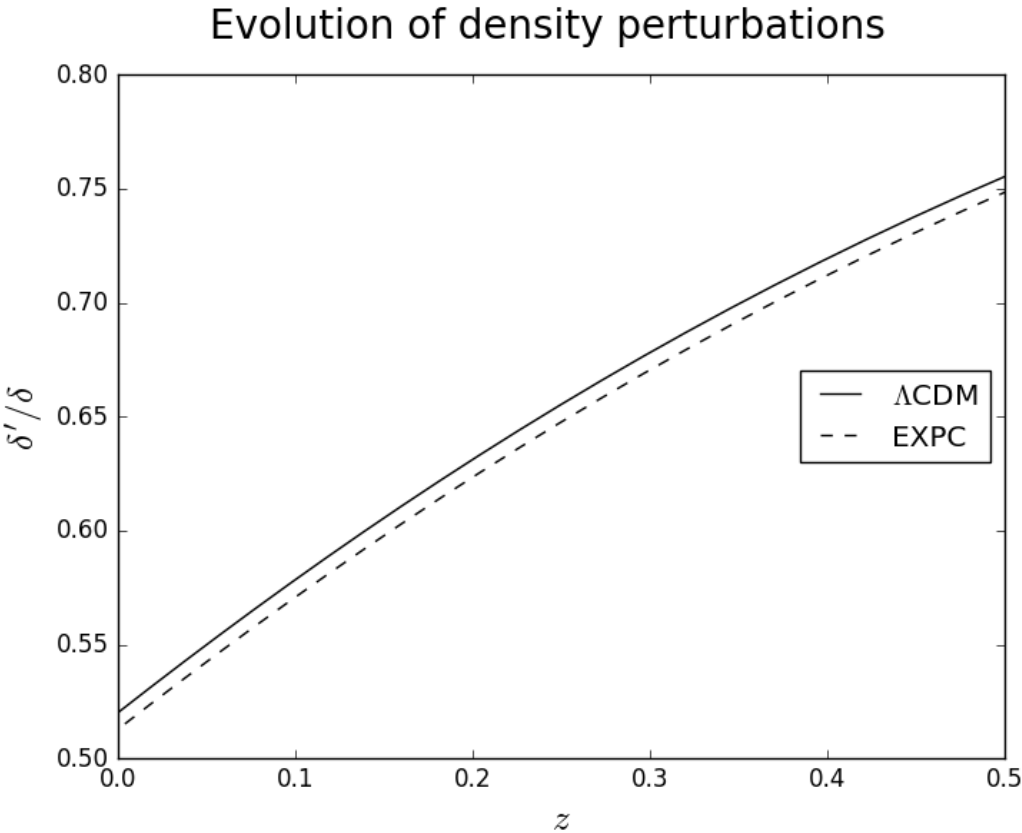
Figure 4.8: This plot shows a closer view of the evolution of the growth factor $\frac{\delta'}{\delta}$ in ΛCDM and EXPC.

CHAPTER 5

Conclusion

In this dissertation, we began by looking at the general cosmological description of our Universe and how, over time, observational data has come to rule in or rule out certain ideas about its evolution and the behaviour of its many components. In particular, we looked at the role of the cosmological constant as dark energy in the standard model of cosmology, ΛCDM, and how dynamical dark energy models work as an alternative.

In Chapter 4, we considered four different dynamical dark energy models and found the one which most closely matched observational data, the coupled exponential potential quintessence model. Using a chi squared test, we found that this model is a better fit for our dataset of 36 values of $H(z)$ than ΛCDM, corroborating similar findings by other studies [66–70], but this result may be skewed due to a systematic error in the observational data.

So what now for the future of dark energy? Are we likely to see the cosmological constant removed from the Einstein equations once more? It is perhaps too early to say, but the observational evidence for dynamical dark energy continues to increase [85]. With upcoming surveys such as DESI and Euclid [71, 86], we will be able to further constrain observational parameters like H_0, and therefore the task of distinguishing between a cosmological constant and dynamical dark energy will become far, far easier.

Regardless of which is the correct picture (and we must remember, there are many more theories about what dark energy is beyond the two considered here– see, for example, the review by Joyce, Lombriser and Schmidt [87] and references therein for more on alternative theories), we can be confident that the phenomenological approach of combining theory and observation will serve the field of cosmology well into the future.

Code Listing

Listing A.1: This listing shows the code written to solve the background equations and perform the chi squared test in the coupled exponential quintessence model.

```python
# -*- coding: utf-8 -*-
"""
Created on Wed May 03 12:40:40 2017

@author: Natalie

This Python script solves the background equations for the coupled exponential
    quintessence model and the LambdaCDM model of dark energy.
It takes a range of initial conditions for the model parameters and prints the results
    that are within 1sigma of the Planck 2015 observational
data to a .csv file. It also calculates a chi squared value on every result for three
    datasets, so that a chi squared test can be performed.
"""

import numpy as np
import matplotlib.pyplot as plt
from scipy import integrate

# DATA #
# we firstly write the list of 36 data points from Zheng et al. 2016 which will be used
    later on
# the x values are redshifts
# the y values are the Hubble parameter at those redshifts
# we also have the uncertainties from the same paper
Zheng_data = [(0.07, 69),(0.09, 69), (0.12, 68.6), (0.17, 83),(0.1791,75),(0.1993, 75),
    (0.2, 72.9), (0.27, 77), (0.28, 88.8),(0.35, 82.7),(0.3519, 83), (0.3802,83),(0.4,
    95),(0.4004, 77),(0.4247,87.1),(0.44, 82.6),(0.4497, 92.8),(0.4783, 80.9),(0.48, 97)
    ,(0.57, 92.9),(0.5929, 104),  (0.6, 87.9),(0.6797, 92),(0.73, 97.3),(0.7812, 105)
    ,(0.8754, 125), (0.88, 90), (0.9, 117), (1.037, 154), (1.3, 168),(1.363, 160),(1.43,
    177), (1.53, 140), (1.75, 202),(1.965, 186.5),(2.34, 222)]

Zheng_uncertainties = [19.6, 12, 26.2, 8, 4, 5, 29.6, 14, 36.6,  8.4, 14, 13.5, 17,
    10.2, 11.2, 7.8, 12.9, 9, 62, 7.8, 13, 6.1, 8, 7, 12,17,40, 23, 20, 17, 33.6, 18, 14,
     40, 50.4, 7]

# the DA and BAO datasets are subsets of the Zheng data
# we write them separately for the different chi sq tests
DA_data = [(0.07, 69), (0.09, 69), (0.12, 68.6), (0.17, 83), (0.1791,75), (0.1993, 75),
    (0.2, 72.9), (0.27, 77), (0.28, 88.8),(0.3519, 83), (0.3802,83), (0.4, 95),(0.4004,
    77), (0.4247,87.1),(0.4497, 92.8),(0.4783, 80.9),(0.48, 97), (0.5929, 104),(0.6797,
```

```python
    92),(0.7812, 105),(0.8754, 125), (0.88, 90),(0.9, 117),(1.037, 154),(1.3, 168)
    ,(1.363, 160),(1.43, 177), (1.53, 140), (1.75, 202),(1.965, 186.5)]

DA_uncertainties = [19.6, 12, 26.2, 8, 4, 5, 29.6, 14, 36.6, 14, 13.5, 17, 10.2, 11.2,
    7.8, 12.9, 9, 62, 13, 8, 12, 17, 40, 23, 20, 17, 33.6, 18, 14, 40, 50.4]

BAO_data = [(0.35, 82.7), (0.44, 82.6), (0.57, 92.9), (0.6, 87.9), (0.73, 97.3), (2.34,
    222)]

BAO_uncertainties = [8.4, 7.8, 7.8, 6.1, 7, 7]

xs = [x[0] for x in Zheng_data]
ys = [x[1] for x in Zheng_data]

xs_DA = [x[0] for x in DA_data]
ys_DA = [x[1] for x in DA_data]

xs_BAO = [x[0] for x in BAO_data]
ys_BAO = [x[1] for x in BAO_data]

# INITIAL CONDITIONS #
# set the initial and final redshifts
z_ini = 100
z_final = 0

# convert this to e-fold numbers N_ini and N_final
N_ini = -np.log(1 + z_ini)
N_final = -np.log(1 + z_final)
timesteps = 250

# calculate the critical density
h = 0.678    # Hubble parameter today in units of 100 km/s/Mpc (Planck 2015)

rho_cr0 = 8.0992*(h**2)*10**(-47) / (2.435*10**18)**4

# calculate the matter density today
Omega_m = 0.3

rho_m0 = Omega_m*rho_cr0

rho_ini = rho_m0*np.exp(3.0*(N_final - N_ini))     # initial value for the matter density
    in terms of N

phi_ini = 0.135     # initial value of phi

phi_pr_ini = 0.0   # initial value of phi'

N = np.linspace(N_ini, N_final, timesteps)

# transform the ts array into a new array containing the z values:
redshift = np.exp(-N) - 1

# open and write headings to csv file
file = open("full_chisq_results.csv",'w')
file.write('beta,lamb,V0,H0,Om0,w0,chisq_lcdm, chisq\n')

# BACKGROUND EQUATIONS #
for beta in np.arange(0.0, 0.06, 0.01):
```

```python
for lamb in np.arange(0.1,1.0,0.01):
    for V0 in np.arange(0.5, 1.1, 0.01):

        def background_eq(y, t): # y[0] = phi, y[1] = phi', y[2] = rho_m

            V = V0*np.exp(-lamb*y[0])

            Vpr = -lamb*V # dV/dphi

            Hsq = (y[2] + V)/(3.0 - 0.5*y[1]**2.0)

            HdotoH2 = - 0.5*y[1]**2.0 - 0.5*y[2]/Hsq

            yprime0 = y[1]

            yprime1 = -(3.0 + HdotoH2)*y[1] - Vpr/Hsq - beta*y[2]/Hsq

            yprime2 = y[2]*(beta*y[1] - 3.0)

            yprime = [yprime0,yprime1,yprime2]

            return yprime

        # solve the background eqns
        y_initial = [phi_ini, phi_pr_ini, rho_ini]

        y = integrate.odeint(background_eq, y_initial, N)

        # calculate the Hubble expansion rate
        V = (V0*10**(-120))*np.exp(-lamb*y[:,0])

        Hubble = np.sqrt((y[:,2] + V)/(3.0 - 0.5*y[:,1]**2.0))

        rhocritical = 3.0*Hubble**2.0

        Omega_matter = y[:,2]/rhocritical

        Omega_phi = (0.5*(y[:,1]*Hubble)**2 + V) / rhocritical

        # convert H to units of km/s/Mpc
        converted_Hubble = np.sqrt((y[:,2] + V)/(3.0 - 0.5*y[:,1]**2.0) )
            /(8.7579*10**(-61))*100

        # define H for LCDM
        H_0 = 67.8 # Planck 2015

        H_lcdm = H_0*((np.sqrt((0.27*(1+redshift)**3) + 0.73)))

        # define the equation of state of dark energy
        w_phi = (0.5*(y[:,1]*Hubble)**2 - V) / (0.5*(y[:,1]*Hubble)**2 + V)

        # find and print the final values
        length = len(Hubble)

        converted_Hubble_final = converted_Hubble[length-1]
        Omega_matter_final = Omega_matter[length-1]
        w_phi_final = w_phi[length-1]
```

```python
# CHI SQUARED TEST #
# create these for chi sq test
Hubble_tuple = np.array(sorted(zip(redshift, converted_Hubble)))
H_lcdm_tuple = np.array(sorted(zip(redshift, H_lcdm)))

# cubic spline interpolation to get values for chi squared test
def cubicSplineSetup(t, y):
    h = np.diff(t)
    b = np.diff(y)/h
    u, v = np.empty(t.size-1), np.empty(t.size-1)
    u[1] = 2.*(h[0]+h[1])
    v[1] = 6.*(b[1]-b[0])
    for i in range(2,t.size-1):
        u[i] = (2.*(h[i]+h[i-1]))-((h[i-1]**2.)/u[i-1])
        v[i] = (6.*(b[i]-b[i-1]))-((h[i-1]*v[i-1])/u[i-1])
    z = np.zeros(t.size)
    l = range(1,t.size-1)
    l.reverse()
    for i in l:
        z[i] = (v[i]-(h[i]*z[i+1]))/u[i]
    A = np.diff(z)/(6.*h)
    B = .5*z[:-1]
    C = b-(h/3.)*(.5*z[1:]+z[:-1])
    return A, B, C

def cubicSplineAt(x, t, y, A, B, C):
    def _interp(i):
        q = x-t[i]
        return A[i]*(q**3.)+B[i]*(q**2.)+C[i]*q+y[i]
    for i in range(t.size-2):
        if x<=t[i+1]:
            return _interp(i)
    return _interp(t.size-2)

def interpolateOverThese(x, t, y, interp=cubicSplineAt, interpSetup=None):
    n = x.size
    f = np.empty(n)
    if interpSetup!=None:
        v = interpSetup(t, y)
        if type(v)==list or type(v)==tuple:
            for i in range(n):
                f[i] = interp(x[i], t, y, *v)
        else:
            for i in range(n):
                f[i] = interp(x[i], t, y, v)
    else:
        for i in range(n):
            f[i] = interp(x[i], t, y)
    return f

# choose Zheng_data, DA_data or BAO_data
x = np.array([i[0] for i in Zheng_data])
f_obs = np.array([i[1] for i in Zheng_data])

t = np.array([i[0] for i in Hubble_tuple])
y = np.array([i[1] for i in Hubble_tuple])

t_lcdm = np.array([i[0] for i in H_lcdm_tuple])
```

```
            y_lcdm = np.array([i[1] for i in H_lcdm_tuple])

            f_int_quintessence = interpolateOverThese(x, t, y,
                                      interp=cubicSplineAt,
                                      interpSetup=cubicSplineSetup)

            f_int_lcdm = interpolateOverThese(x, t_lcdm, y_lcdm,
                                      interp=cubicSplineAt,
                                      interpSetup=cubicSplineSetup)

            # chi squared tests
            chi_squared = sum(((f_obs-f_int_quintessence)**2)/f_int_quintessence)
            chi_squared_lcdm = sum(((f_obs-f_int_lcdm)**2)/f_int_lcdm)
            # alter number of rows according to dataset chosen
            rows = 35
            columns = 2
            deg_of_freedom = (rows-1)*(columns-1)

# if/ else excludes results outside 1sigma of observational data (Planck 2015)
            if 66.9<= converted_Hubble_final <= 68.7:
                if 0.296 <= Omega_matter_final <= 0.32:
                    if -1.051 <= w_phi_final <= -0.961:
                        # results written to the file opened earlier
                        file.write('{},{},{},{},{},{}, {}, {}\n'.format(beta, lamb, V0,
                            converted_Hubble_final, Omega_matter_final, w_phi_final,
                            chi_squared_lcdm, chi_squared))
            else:
                pass

# close the file
file.close()

# PLOTS #
# compare the evolution of H in LCDM and quintessence with Zheng data
fig = plt.figure()
plt.plot(redshift, H_lcdm, linestyle='-', color= 'k', label='$\Lambda$CDM')
plt.plot(redshift, converted_Hubble, linestyle='--', color='k', label='EXPC')
plt.errorbar(xs,ys, yerr=Zheng_uncertainties, linestyle='none', color='k', marker='x',
    label='Data points from \nZheng et al. (2016)')
fig.suptitle('Evolution of $H(z)$ in $\Lambda$CDM and EXPC', fontsize=18)
plt.xlabel('$z$', fontsize=18)
plt.ylabel('$H(z)$ (kms$^{-1}$Mpc$^{-1}$)', fontsize=18)
plt.xlim(0,1)
plt.ylim(30,160)
plt.legend(loc='upper left', fontsize=10)

# compare the evolution of Omega matter and Omega phi
fig = plt.figure()
plt.plot(redshift, Omega_matter, linestyle='-', color='k', label='$\Omega_{m}$')
plt.plot(redshift, Omega_phi, linestyle ='--', color='k', label='$\Omega_{\phi}$')
fig.suptitle('Evolution of $\Omega_{m}$ and $\Omega_{\phi}$ in EXPC', fontsize=20)
plt.xlabel('$z$', fontsize=18)
plt.xlim(0,5)
plt.legend(loc='center right')

# the evolution of w as a function of z
fig = plt.figure()
plt.plot(redshift, w_phi, color='k', label='$w$')
```

```
fig.suptitle('Evolution of the equation of state $w$ in EXPC', fontsize=18)
plt.xlabel('$z$', fontsize=18)
plt.ylabel('$w$', fontsize=18)
plt.xlim(0,5)
plt.ylim(-1,-0.99)
plt.legend(loc='upper left')

plt.show()
```

Bibliography

[1] A. G. Riess et al. Observational Evidence from Supernovae for an Accelerating Universe and a Cosmological Constant. *The Astronomical Journal*, 116:1009–1038, September 1998.

[2] S. Perlmutter et al. Measurements of Ω and Λ from 42 High-Redshift Supernovae. *The Astrophysical Journal*, 517:565–586, June 1999.

[3] A. Einstein. Die Grundlage der allgemeinen Relativitätstheorie [The Foundation of the General Theory of Relativity]. *Annalen der Physik*, 354:769–822, 1916.

[4] A. Friedmann. Über die Krümmung des Raumes [On the Curvature of Space]. *Zeitschrift für Physik*, 10:377–386, 1922.

[5] E. Hubble. A Relation between Distance and Radial Velocity among Extra-Galactic Nebulae. *Proceedings of the National Academy of Science*, 15:168–173, March 1929.

[6] E. J. Copeland, M. Sami, and S. Tsujikawa. Dynamics of Dark Energy. *International Journal of Modern Physics D*, 15(11):1753–1935, 2006.

[7] L. Amendola and S. Tsujikawa. *Dark Energy: Theory and Observations*. Cambridge University Press, 2010.

[8] S. Chandrasekhar. The Maximum Mass of Ideal White Dwarfs. *The Astrophysical Journal*, 74:81, July 1931.

[9] D. N. Spergel et al. First–Year Wilkinson Microwave Anisotropy Probe (WMAP) Observations: Determination of Cosmological Parameters. *Astrophysical Journal Supplement*, 148:175–194, September 2003.

[10] D. N. Spergel et al. Three–Year Wilkinson Microwave Anisotropy Probe (WMAP) Observations: Implications for Cosmology. *Astrophysical Journal Supplement*, 170:377–408, June 2007.

[11] G. Hinshaw et al. Five–Year Wilkinson Microwave Anisotropy Probe Observations: Data Processing, Sky Maps, and Basic Results. *Astrophysical Journal Supplement*, 180:225–245, February 2009.

[12] P. Astier et al. The Supernova Legacy Survey: measurement of Ω_M, Ω_Λ and w from the first year data set. *Astronomy & Astrophysics*, 447:31–48, February 2006.

[13] A. G. Riess et al. New Hubble Space Telescope Discoveries of Type Ia Supernovae at $z = 1$: Narrowing Constraints on the Early Behavior of Dark Energy. *The Astrophysical Journal*, 659:98–121, April 2007.

[14] W. M. Wood–Vasey et al. Observational Constraints on the Nature of Dark Energy: First Cosmological Results from the ESSENCE Supernova Survey. *The Astrophysical Journal*, 666:694–715, September 2007.

[15] E. Carretta et al. Distances, Ages, and Epoch of Formation of Globular Clusters. *The Astrophysical Journal*, 533:215–235, April 2000.

[16] Planck Collaboration. Planck 2015 results. XIII. Cosmological parameters. *Astronomy & Astrophysics*, 594, September 2016.

[17] J.-F. Dufaux. Gravity Waves from the Nonperturbative Decay of Condensates along Supersymmetric Flat Directions. *Physical Review Letters*, 103(4):041301, July 2009.

[18] B. P. Abbott et al. Observation of Gravitational Waves from a Binary Black Hole Merger. *Physical Review Letters*, 116(6):061102, February 2016.

[19] A. A. Penzias and R. W. Wilson. A Measurement of Excess Antenna Temperature at 4080 Mc/s. *The Astrophysical Journal*, 142:419–421, July 1965.

[20] G. F. Smoot et al. Structure in the COBE differential microwave radiometer first–year maps. *The Astrophysical Journal Letters*, 396:L1–L5, September 1992.

[21] P. de Bernardis et al. A Flat Universe from High Resolution Maps of the Cosmic Microwave Background Radiation. *Nature*, 404:955–959, April 2000.

[22] A. Balbi et al. Constraints on Cosmological Parameters from MAXIMA-1. *The Astrophysical Journal Letters*, 545(1):L1, May 2000.

[23] P. Peter and J.-P. Uzan. *Primordial Cosmology*. Oxford Graduate Texts, 2013.

[24] M. Kamionkowski, D. N. Spergel, and N. Sugiyama. Small–scale cosmic microwave background anisotropies as probe of the geometry of the universe. *Astrophysical Journal Letters*, 426:57–60, May 1994.

[25] S. Weinberg. Curvature dependence of peaks in the cosmic microwave background distribution. *Physical Review D*, 62(12):127302, December 2000.

[26] G. Hinshaw et al. Three-Year Wilkinson Microwave Anisotropy Probe (WMAP) Observations: Temperature Analysis. *The Astrophysical Journal Supplement*, 170:288–334, June 2007.

[27] N. Kaiser. Lecture notes: Elements of Astrophysics. `https://www.ifa.hawaii.edu/~kaiser/lectures/`, April 2002. Accessed 07/04/17.

[28] W. J. Percival et al. Measuring the Baryon Acoustic Oscillation scale using the Sloan Digital Sky Survey and 2dF Galaxy Redshift Survey. *Monthly Notices of the Royal Astronomical Society*, 381:1053–1066, November 2007.

[29] Astronomy Magazine. Does dark energy really exist? `http://www.astronomy.com/news/2003/12/does-dark-energy-really-exist`, 2003. Accessed 10/12/16.

[30] T. Clifton and P. G. Ferreira. Does Dark Energy Really Exist? *Scientific American*, 300:48–55, April 2009.

[31] Phys.org. The universe is expanding at an accelerating rate– or is it? `http://phys.org/news/2016-10-universe-rateor.html`, 2016. Accessed 10/12/16.

[32] T. Mattsson. Dark energy as a mirage. *General Relativity and Gravitation*, 42:567–599, March 2010.

[33] M. Ishak et al. Dark energy or apparent acceleration due to a relativistic cosmological model more complex than the Friedmann–Lemaitre–Robertson–Walker model? *Physical Review D*, 78(12), December 2008.

[34] V. Marra et al. Cosmological observables in a Swiss–cheese universe. *Physical Review D*, 76(12):123004, December 2007.

[35] J. T. Nielsen, A. Guffanti, and S. Sarkar. Marginal evidence for cosmic acceleration from Type Ia supernovae. *Scientific Reports*, 6:35596, October 2016.

[36] M. Betoule et al. Improved cosmological constraints from a joint analysis of the SDSS–II and SNLS supernova samples. *Astronomy & Astrophysics*, 568:A22, August 2014.

[37] E.A. Milne. *Relativity, Gravitation, and World–Structure*. Oxford Clarendon Press, 1935.

[38] D. Rubin and B. Hayden. Is the expansion of the universe accelerating? All signs point to yes. arXiv:1610.08972, October 2016.

[39] H. I. Ringermacher and L. R. Mead. In Defense of an Accelerating Universe: Model Insensitivity of the Hubble Diagram. arXiv:astro-ph/1611.00999, November 2016.

[40] V. V. Luković, R. D'Agostino, and N. Vittorio. Is there a concordance value for H_0? *Astronomy & Astrophysics*, 595:A109, November 2016.

[41] B. S. Haridasu et al. Strong evidence for an accelerating universe. *Astronomy & Astrophysics*, 600:L1, February 2017.

[42] G. Weinstein. George Gamow and Albert Einstein: Did Einstein say the cosmological constant was the "biggest blunder" he ever made in his life? arXiv:1310.1033, 2013.

[43] V. M. Slipher. The radial velocity of the Andromeda Nebula. *Lowell Observatory Bulletin*, 2:56–57, October 1913.

[44] S. Weinberg. The cosmological constant problem. *Reviews of Modern Physics*, 61:1–23, January 1989.

[45] S. M. Carroll. The Cosmological Constant. *Living Reviews in Relativity*, 4, December 2001.

[46] J. Martin. Everything you always wanted to know about the cosmological constant problem (but were afraid to ask). *Comptes Rendus Physique*, 13:566–665, July 2012.

[47] H. Casimir. On the attraction between two perfectly conducting plates. *Proceedings of the Royal Netherlands Academy of Arts and Sciences*, 51:793–795, May 1948.

[48] P. J. Mohr, D. B. Newell, and B. N. Taylor. CODATA recommended values of the fundamental physical constants: 2014. *Reviews of Modern Physics*, 88:035009, September 2016.

[49] B. Carter. Large number coincidences and the anthropic principle in cosmology. In *Confrontation of Cosmological Theories with Observational Data*, volume 63 of *IAU Symposium*, pages 291–298, September 1974.

[50] J.D. Barrow and F.J. Tipler. *The Anthropic Cosmological Principle*. Oxford University Press, 1988.

[51] S.M. Carroll. Lecture notes: The preposterous Universe. `https://ned.ipac. caltech.edu/level5/March01/Carroll/Carroll1.html`, 2001. Accessed 11/12/16.

[52] N. Sivanandam. Is the cosmological coincidence a problem? *Physical Review D*, 87(8), April 2013.

[53] H. E. S. Velten, R. F. vom Marttens, and W. Zimdahl. Aspects of the cosmological "coincidence problem". *European Physical Journal C*, 74, November 2014.

[54] E. Bianchi and C. Rovelli. Why all these prejudices against a constant? arXiv:1002.3966, February 2010.

[55] P. J. Steinhardt, L. Wang, and I. Zlatev. Cosmological tracking solutions. *Physical Review D*, 59(12):123504, June 1999.

[56] T. Padmanabhan. Dark Energy: Mystery of the Millennium. In *Albert Einstein Century International Conference*, volume 861 of *American Institute of Physics Conference Series*, pages 179–196, November 2006.

[57] M. F. Sohnius. Introducing supersymmetry. *Physics Reports*, 128:39–204, November 1985.

[58] B. Ratra and P. J. E. Peebles. Cosmological consequences of a rolling homogeneous scalar field. *Physical Review D*, 37:3406–3427, June 1988.

[59] C. Wetterich. Quintessence – the Dark Energy in the Universe? *Space Science Reviews*, 100(1), January 2002.

[60] L. Amendola. Coupled quintessence. *Physical Review D*, 62(4):043511, August 2000.

[61] A. W. Brookfield, C. van de Bruck, and L. M. H. Hall. New interactions in the dark sector mediated by dark energy. *Physical Review D*, 77(4):043006, February 2008.

[62] G.-B. Zhao et al. Examining the Evidence for Dynamical Dark Energy. *Physical Review Letters*, 109(17):171301, October 2012.

[63] H.-J. Seo and D. J. Eisenstein. Probing Dark Energy with Baryonic Acoustic Oscillations from Future Large Galaxy Redshift Surveys. *The Astrophysical Journal*, 598:720–740, December 2003.

[64] R. Jimenez and A. Loeb. Constraining cosmological parameters based on relative galaxy ages. *The Astrophysical Journal*, 573:37–42, July 2002.

[65] V. Sahni et al. Statefinder– A new geometrical diagnostic of dark energy. *Soviet Journal of Experimental and Theoretical Physics Letters*, 77:201–206, March 2003.

[66] V. Sahni, A. Shafieloo, and A. A. Starobinsky. Model–independent Evidence for Dark Energy Evolution from Baryon Acoustic Oscillations. *The Astrophysical Journal Letters*, 793:L40, October 2014.

[67] X. Ding et al. Is There Evidence for Dark Energy Evolution? *The Astrophysical Journal Letters*, 803:L22, April 2015.

[68] X. Zheng et al. What are the $Omh^2(z1, z2)$ and $Om(z1, z2)$ diagnostics telling us in light of $H(z)$ data? *The Astrophysical Journal*, 825(1):17, June 2016.

[69] J.-Z. Qi, M.-J. Zhang, and W.-B. Liu. Testing dark energy models with $H(z)$ data. arXiv:1606.00168, June 2016.

[70] Y. Zhang et al. Probing dynamics of dark energy with latest observations. arXiv:1703.08293, March 2017.

[71] M. Levi et al. The DESI Experiment, a whitepaper for Snowmass 2013. arXiv:1308.0847, August 2013.

[72] DESI Survey. Dark Energy Spectroscopic Instrument. `http://desi.lbl.gov/`, 2017. Accessed 12/04/17.

[73] J. Weller and A. Albrecht. Future supernovae observations as a probe of dark energy. *Physical Review D*, 65(10):103512, May 2002.

[74] V. Pettorino et al. Constraints on coupled dark energy using CMB data from WMAP and South Pole Telescope. *Physical Review D*, 86(10):103507, November 2012.

[75] L. Amendola and C. Quercellini. Tracking and coupled dark energy as seen by the Wilkinson Microwave Anisotropy Probe. *Physical Review D*, 68:023514, July 2003.

[76] V. Bonvin et al. H0LiCOW - V. New COSMOGRAIL time delays of HE 0435-1223: H_0 to 3.8% precision from strong lensing in a flat ΛCDM model. *Monthly Notices of the Royal Astronomical Society*, 465:4914–4930, March 2017.

[77] A. G. Riess et al. A 2.4% Determination of the Local Value of the Hubble Constant. *The Astrophysical Journal*, 826:56, July 2016.

[78] J. N. Grieb et al. The clustering of galaxies in the completed SDSS-III Baryon Oscillation Spectroscopic Survey: Cosmological implications of the Fourier space wedges of the final sample. *Monthly Notices of the Royal Astronomical Society*, 467:2085–2112, May 2017.

[79] E. Di Valentino et al. Constraining Dark Energy Dynamics in Extended Parameter Space. arXiv:1704.00762, April 2017.

[80] S. Tsujikawa. Lecture notes: Introductory review of cosmic inflation. arXiv:hep-ph/0304257, April 2003.

[81] NIST/SEMATECH. e-Handbook of Statistical Methods. `http://www.itl.nist.gov/div898/handbook/eda/section3/eda3674.htm`, October 2013. Accessed 14/04/17.

[82] A. Lewis and A. Challinor. Code for Anisotropies in the Microwave Background. `http://camb.info/`, 2017. Accessed 13/05/17.

[83] D. Blas, J. Lesgourgues, and T. Tram. The Cosmic Linear Anisotropy Solving System. `http://class-code.net/`, 2017. Accessed 13/05/17.

[84] J. C. Fabris, S. V. B. Goncalves, and P. E. de Souza. Density perturbations in an Universe dominated by the Chaplygin gas. *General Relativity and Gravitation*, 34(1):53–63, March 2001.

[85] G.-B. Zhao et al. The clustering of galaxies in the completed SDSS-III Baryon Oscillation Spectroscopic Survey: Examining the observational evidence for dynamical dark energy. arXiv:1701.08165, January 2017.

[86] R. Laureijs et al. Euclid: ESA's mission to map the geometry of the dark universe. In *Space Telescopes and Instrumentation 2012: Optical, Infrared, and Millimeter Wave*, volume 8442 of *Proceedings of the SPIE*, page 84420T, September 2012.

[87] A. Joyce, L. Lombriser, and F. Schmidt. Dark Energy Versus Modified Gravity. *Annual Review of Nuclear and Particle Science*, 66:95–122, October 2016.